Here

SOUTHEASTERN GEOLOGY

PUBLISHED AT DUKE UNIVERSITY DURHAM, NORTH CAROLINA

VOL. 11 NO. 1 NOVEMBER, 1969

SOUTHEASTERN GEOLOGY

PUBLISHED QUARTERLY

AT

DUKE UNIVERSITY

This journal welcomes original papers on all phases of geology, geophysics, and geochemistry as related to the Southeast. Transmit manuscripts to S. DUNCAN HERON, JR., BOX 6665, COLLEGE STATION, DURHAM, NORTH CAROLINA. Please observe the following:

(1) Type the manuscript with double space lines and submit in duplicate.
(2) Cite references and prepare bibliographic lists in accordance with the method found within the pages of this journal.
(3) Submit line drawings and complex tables as finished copy.
(4) Make certain that all photographs are sharp, clear, and of good contrast.
(5) Stratigraphic terminology should abide by the Code of Stratigraphic Nomenclature (AAPG, v. 45, 1961).

Proofs will not be sent authors unless a request to this effect accompanies the manuscript.

Reprints must be ordered prior to publication. Prices are available upon request.

* * * * * *

Subscriptions to Southeastern Geology are $5.00 per volume. Inquiries should be addressed to WM. J. FURBISH, BUSINESS AND CIRCULATION MANAGER, BOX 6665, COLLEGE STATION, DURHAM NORTH CAROLINA. Make check payable to Southeastern Geology.

SOUTHEASTERN GEOLOGY

Table of Contents

Vol. 11, No. 1

1969

ALPHA-AUTORADIOGRAPHY AND MORPHOLOGY OF ACCESSORY ZIRCON SUITES

By

Paul C. Ragland
Department of Geology
University of North Carolina
Chapel Hill, North Carolina

ABSTRACT

Zircons were separated from five bentonites and a variety of other rocks, after which they were studied by α-autoradiography and standard petrographic techniques. Differences in elongation, rounding, and dispersion of size distributions were found to be useful to distinguish between the various zircon suites. Evidence is offered to demonstrate that: (1) zircons from the five bentonites are apparently from a homogeneous population; (2) U^{4+} and Th^{4+} can occupy regular lattice positions in zircon; and (3) zircons with complex crystal habits are in general smaller than those with less complex habits. Monazite or other highly radioactive impurities, which if present generally make up less than two percent of the zircon suite, can account for more than 50 percent of the radioactivity.

INTRODUCTION

The studies described below were originally undertaken at Rice University as part of a program to date bentonites by the isotopic analysis of the uranium and lead in zircon separated from bentonites. The autoradiographic, petrologic, and mineralogical studies were designed to get some insight into two fundamental questions: 1) What criteria can be used to define a suite of zircon minerals as belonging to one population formed at one time in one geologic environment? 2) What criteria can be applied to define a closed system in the geochronological sense? Some authors conclude that the high precision obtained on the various absolute ages determined on zircon suites separated from Middle Ordovician bentonites (Adams and Rogers, 1961, Adams, et al., 1960) is due in large part to the techniques and selection criteria described here.

The purpose of this paper, therefore, is (1) to compare α-autoradiography with morphologic studies as a means of characterizing a zircon suite, and (2) to determine the site of the α-emitters in zircons

by autoradiography. Studies of zircon morphology are numerous. Poldervaart and his co-workers, for example, have published several articles concerning zircon morphology and its application to petrogenetic problems (see Poldervaart, 1955, 1956; Poldervaart and Eckelmann, 1955; Larsen and Poldervaart, 1957; Alper and Poldervaart, 1957). This study utilizes some of their techniques to determine the relationship between zircon morphology and radioactivity.

Considerable information is available concerning the total α-activity of zircon suites (e. g., Jaffe, et al., 1959) as well as U and Th analyses of zircon suites (Hurley and Fairbairn, 1957; Ahrens, 1965). Few data are available, however, concerning the site of the α-emitters within an individual zircon crystal. Silver and Deutsch (1963) utilized the autoradiographic method and some leaching experiments and have provided considerable quantitative data on the site of U and Th in zircon. It is commonly thought, though not proven, that U and Th exist in solid solution, occupying Zr lattice sites in the crystal. However, much of the U and Th in felsic igneous rocks has been demonstrated to be readily leachable by dilute acid, implying that there are other sites than lattice positions in accessory minerals. McIntire (1963) has pointed out that in the case of solid solution, autoradiographs should yield a uniform track density over the crystal, whereas in the case of occlusion, tracks might be concentrated along certain planes or in patches. Other possible sites exist, for the fact that much of the radioactivity is readily leachable implies that secondary crack fillings and coatings, normally an opaque material resembling hematite or limonite, may be highly radioactive. In addition, zircon crystals commonly have many inclusions, which may be comparatively radioactive. This paper hopefully will answer some of these questions as well as present some new information concerning zircon morphology.

Acknowledgments

The writer is indebted to Mrs. Lynn Davis Pollard for her aid in collecting the data. John J. W. Rogers and Knut S. Heier kindly reviewed the manuscript. John A. S. Adams supplied some of the samples and provided help and encouragement throughout the project. A portion of the research was sponsored by the Robert A. Welch Foundation Grant C-009 to John A. S. Adams and John J. W. Rogers.

PROCEDURE

Zircons were separated from 10 samples by means of the standard procedures, heavy liquids (bromoform and methylene iodide) and the Frantz isodynamic separator. Sample descriptions and localities are given in Table 1. The bentonites needed very little crushing, for they usually could be disaggregated by elutriation in a large tank of

Table 1. Sample Localities.

Sample	Rock Type	Locality	Age	Stratigraphy	Reference
KIN-2	bentonite	Kinnekule, Sweden	Middle Ordovician	Chasmops Series, Caradocian	Bystrom-Asklund et al. (1961)
GH-12	bentonite	Roane Co., Tenn., USA	Middle Ordovician	Chicamauga Ls.	Hammil (1957)
JHT-8	bentonite	Culberson Co. Texas, USA	Permian Guadalupian	Manzanita Member Cherry Canyon Fm.	Terrell (1960)
GH-26	bentonite	Bedford Co., Tenn., USA	Middle Ordovician	Carters Ls., Stones River Group	Wilson (1949)
GH-14	bentonite	Roane Co., Tenn., USA	Middle Ordovician	Chicamauga Ls.	Hammill (1957)
LAU-1	granite	near Dresden, Saxony, E. Germany	Devonian (?)	----------	Schurmann et al. (1956) Hoppe (1965)
PCR-65	amphibolite	Mason Co., Texas, USA	Precambrian	Packsaddle Schist	Ragland (1961)
PCR-25C	granite gneiss	Llano Co., Texas, USA	Precambrian	Red Mountain Gneiss	Boyer and Clabaugh (1959)
PCR-1	quartzofeldspathic gneiss	Mason Co., Texas, USA	Precambrian	Valley Spring Gneiss	Ragland (1961)
FBS-1	beach sand	Florida*, U.S.A.	Recent	----------	----------

*exact location unknown

water. Samples PCR-65, PCR-25C and PCR-1 were passed through a jaw crusher, pulverized to -100 mesh, and elutriated before the zircon separation was performed. Normally 10-50 kilograms of bulk material were processed to obtain one gram of pure zircon.

The problem of breakage of zircons during pulverizing is of concern and should be mentioned. Larsen and Poldervaart (1957) investigated this problem carefully and concluded that there was very little breakage during pulverizing. Such is not the case here, for the relationship between the percent broken crystals and rock type in Table 2 suggests that some crystals are broken during pulverizing. The well-indurated granite and metamorphic rocks received the most vigorous treatment during crushing and the percent broken zircon crystals from these rocks varies from 35-46 percent. With the exception of JHT-8 (39 percent broken zircon crystals) the zircon suites from bentonites contain only 12-18 percent broken crystals. The bentonites were subjected to relatively mild treatment. Moreover, FBS-1, a beach sand, was not pulverized at all and contains only 9 percent broken zircon crystals.

The autoradiographs were prepared by impregnating several hundred zircon crystals in nuclear track plates and pouring a liquid nuclear emulsion over each plate (Ragland, 1964). The plates were

Table 2. Summary Data for Zircon Suites.

Sample Rock Type	KIN-2	GH-12	JHT-8 bentonites	GH-26	GH-14
ave. *length in mm. -l	.099±.040	.166±.041	.101±.026	.134±.054	.110±.050
ave. *breadth in mm.-b	.035±.009	.050±.014	.047±.013	.055±.024	.058±.021
ave. *size - $\sqrt{lb}$	.058±.014	.073±.014	.065±.019	.083±.029	.079±.031
ave. *elongation ratio-b/l	.41±.15	.44±.16	.48±.19	.45±.21	.54±.15
rounding ratio[1]	3.1	11	1.2	2.5	4.8
transparency ratio[2]	5.7	5.9	2.0	5.9	3.7
% broken crystals	16	18	39	12	14
ave.# $\propto/cm^2/sec \times 10^{-2}$	.75	.52	.73	.77	.81

Sample Rock Type	LAU-1 granite	PCR-65 amphibolite	PCR-25C gneiss	PCR-1 gneiss	FBS-1 beach sand
ave. *length in mm. -l	.088±.038	.111±.035	.117±.044	.119±.044	.166±.050
ave. *breadth in mm. -b	.040±.011	.061±.021	.060±.023	.080±.029	.101±.033
ave. *size - $\sqrt{lb}$	.057±.019	.082±.023	.084±.026	.095±.035	.124±.024
ave. *elongation ratio - b/l	.46±.16	.59±.15	.51±.19	.67±.19	.62±.21
rounding ratio[1]	4.0	0.1	19	0.8	0.9
transparency ratio[2]	6.3	0.6	6.2	0.8	3.0
% broken crystals	41	39	35	46	9
ave.# $\propto/cm^2/sec \times 10^{-2}$	1.7	1.2	.45	.20	.49

*average quoted as arithmetic mean ± one standard deviation, (x ± s)
1 average quoted as median value
defined as: $\frac{\text{euhedral crystals + subhedral crystals}}{\text{rounded crystals}}$
[2]defined as: $\frac{\text{transparent crystals + translucent crystals}}{\text{frosted crystals}}$

allowed to expose for a maximum of 59 days before development. The developed slides were placed under a polarizing microscope with a mechanical stage and studied at X210 and X450 magnification. Traverses were made across each slide until a minimum of 100 doubly terminated individual crystals were studied per slide.

Several parameters were measured on each crystal. Length (l) and breadth (b) were measured only on doubly terminated, unbroken crystals. From these measurements, size (the geometric mean, $\sqrt{lb}$), elongation ratio (b/l), and "volume" (b^2xl) were calculated. In order to report the $\propto$ -activity in $\propto/cm^2/sec \times 10^{-2}$, surface area

was calculated on the basis of three prism faces and the upper faces of the pyramids. Alpha-tracks from the bottom faces cannot be seen so these faces were not included in the measurement of surface area. It was also noted whether the crystal was euhedral, subhedral or anhedral, as well as transparent, translucent or opaque. All these data are summarized in Table 2. Crystallographic form was recorded for euhedral and subhedral crystals. Color, presence of outgrowth and/or overgrowths, as well as abundance and nature of inclusions were also noted. The sites of the α-emitters were recorded on the basis of their partition between inclusions, crack fillings, surface coatings and randomly distributed throughout the crystals.

COMPARISON OF ZIRCON SUITES

Of particular interest in this study is the comparison of zircon suites from bentonites with those from other rock types. These GH zircon suites were used for absolute age dating by the U-Pb method (Adams and Rogers, 1961) and one purpose of the present work was to determine whether or not the suite represented one population formed at one time. Bentonites, representing volcanic ash that has been altered largely to montmorillonite clay, are excellent stratigraphic marker beds in that one unit may commonly extend over a wide geographic area and yet be deposited over a very short interval of geologic time. Indeed, a single bentonite may represent one ash fall and the zircons within it a homogeneous population. Ragland (1964) compared the α-activity of zircons from a bentonite with those from a placer sand. He concluded that the zircons from the bentonite represent a single population whereas those from the sand represent multiple populations. Larsen and Poldervaart (1957) point out that the size and elongation of self-nucleating, free-growing crystals is dependent upon their physico-chemical environment, which probably is essentially uniform in a volcanic neck immediately before eruption. Thus it would be expected for zircons in a single ash fall to represent a single, homogeneous population with respect to at least some measured variates.

In addition, zircon suites from bentonites may be compared with those from multiple sources (FBS-1, the beach sand) and with those of questionable origin (PCR-65, PCR-25C, and PCR-1, the metamorphic rocks). Eckelmann and Kulp (1956), for example, concluded that the Cranberry and Henderson "granites" of North Carolina were metasediments based upon their zircon morphologies. Many other studies have discussed the use of zircon morphologies to distinguish between metamorphic rocks and granites of sedimentary as opposed to igneous origin. Saxena (1966) gives a comprehensive review of this literature.

The frequency distributions of the α-activities for each zircon suite are shown in Figure 1 and the average α-activity is given in Table 2. Only "normal" zircons were considered; malacons, hyacinths and

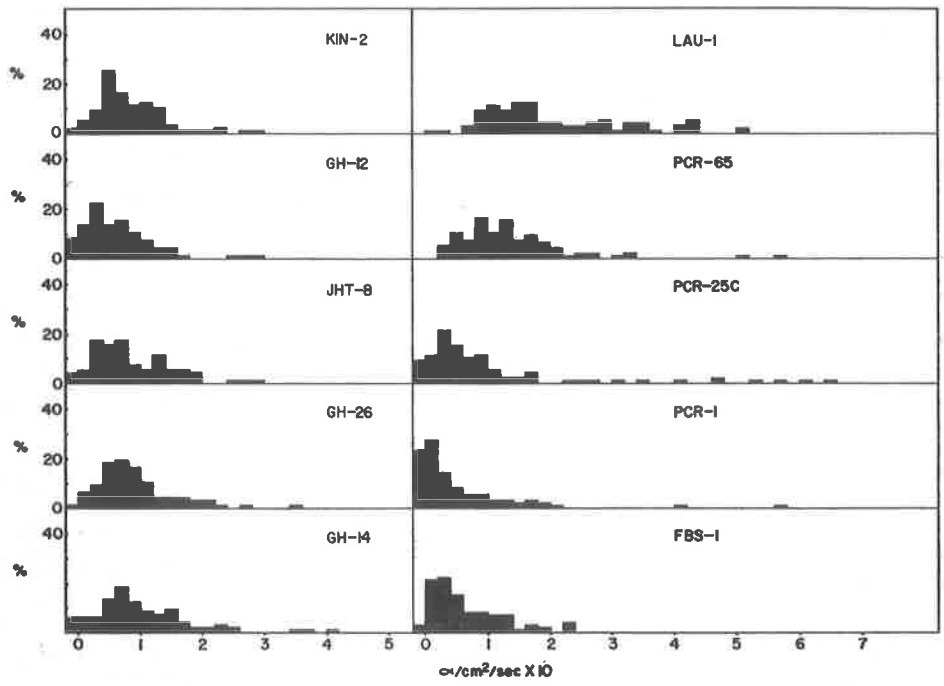

Figure 1. Histograms of ∝-activities.

metamict zircons were not included. Neither the averages nor the relative dispersion of each distribution as shown in the histograms reveals differences between bentonite suites and those from other rock types. With the exception of the zircons from GH-12, averages for bentonite suites are remarkably uniform, varying from 0.73-0.81 ∝/ $cm^2/sec \times 10^{-2}$. However, as a means of characterizing an individual zircon suite and distinguishing it from other suites, the use of ∝-activity distributions was not successful in this study.

Arithmetic means and standard deviations for length, breadth, size and elongation ratio for each sample are listed in Table 2. The data for LAU-1 (Lausitz Granodiorite) are in good agreement with those of Hoppe (1965) and Schurmann et al., (1956). These data are shown graphically in Figure 2, which is a plot of average breadth vs. average length for each suite (represented by the open and closed circles) where the slope of the lines represents the ratio of the respective standard deviations (S_b/S_l). Each line is referred to as a reduced major axis. The application of this concept to zircon studies is discussed in Alper and Poldervaart (1957) and Larsen and Poldervaart (1957). A detailed discussion of the method and calculations is given in Imbrie (1956). The reduced major axis is envisioned as a trend of zircon growth in a particular environment. Note that the majority of the lines would pass reasonably close to the origin, indicating that the crystals are self-

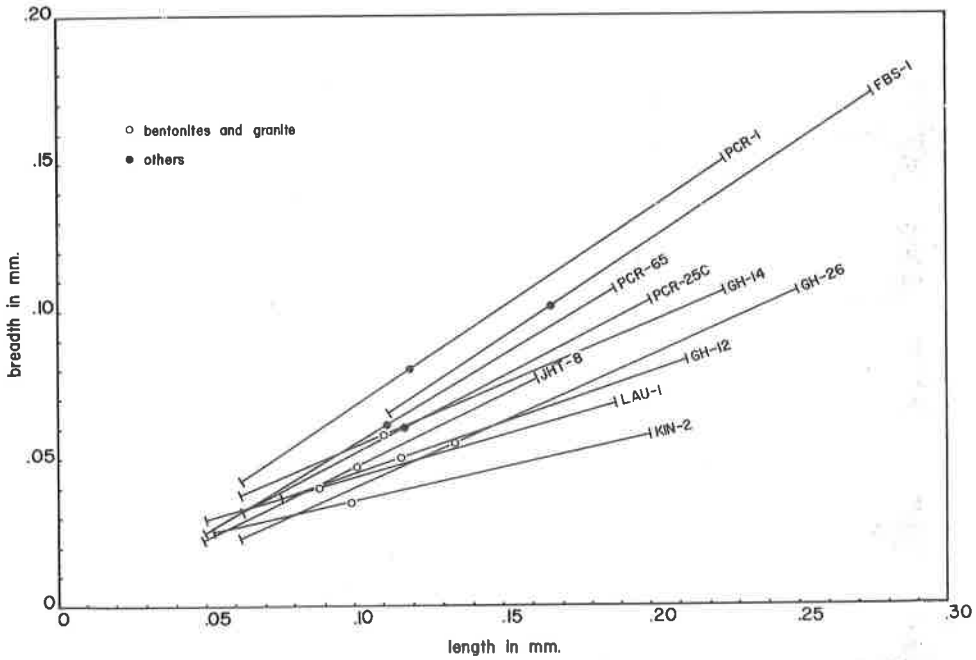

Figure 2. Reduced major axes for the ten zircon suites.

nucleating. The length of the lines are established by graphically eliminating the extreme 2 1/2 percent of the largest and smallest crystals. If the slopes are similar and the points are close together, several statistical tests have been developed to determine differences in zircon suites. These tests are described in the references listed above. Where the reduced major axes are quite different, as they are in Figure 2, visual observations will suffice. Some observations may be made from the data presented in Table 2 and Figure 2:

1. Zircon crystals from the bentonites and granite are generally more acicular, which is in general agreement with the fact that igneous zircons are commonly more acicular than sedimentary zircons, as reported in Poldervaart (1955, 1956).

2. Zircons from the beach sand are considerably larger than those from other rocks, but are still well within the range for zircons from common plutonic rocks Poldervaart, 1956).

3. Unbroken crystals from suites that contain larger grains are on the average more equant than those from suites of smaller grains. Apparently the large, acicular crystals are broken during stream transport or crushing in the laboratory.

4. Dispersion as shown by length of reduced major axes is generally less in the bentonite suites.

This last point was further developed by plotting histograms of "volumes" ($1 \times b^2$) of zircons from the entire suite, including broken crystals. This measurement was found to be much more diagnostic

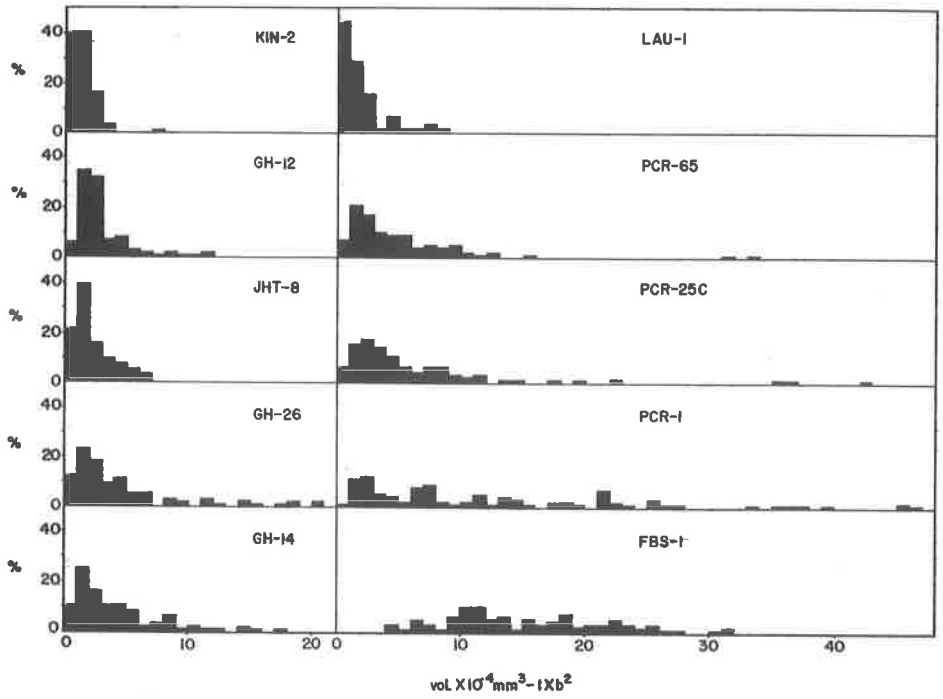

Figure 3. Volume histograms.

than the usual measure of size $\sqrt{lb}$, which is commonly measured only on doubly terminated, unbroken crystals. The larger the dispersion of the volume or size histogram the greater is the chance for multiple populations. These results are shown in Figure 3, which demonstrates a marked difference in frequency distributions of volume. Compare for example, FBS-1, the beach sand concentrate, with any of the bentonite suites in the left column. Of the metamorphic suites, these data indicate that PCR-1 contains several zircon populations and is of probable sedimentary origin, and the others are of questionable origin.

The similarity of the zircon suites from the bentonites in average size, elongation and α-activity suggest that they may represent one homogeneous population; i. e., they all crystallized under similar physicochemical conditions. This hypothesis was tested by plotting cumulative frequency distributions on probability scales for zircons from all five bentonites. A variate may be normally distributed where the cumulative frequency distribution of the raw data plots as a straight line on probability paper. It is said to be lognormally distributed if the cumulative frequency distribution of the logs of the raw data plot as a straight line. The difference between the two distributions can be seen by comparing Figure 4 and 5. Figure 4 indicates that the elongation ratio data (b/l) are normally distributed, whereas Figure 5 indicates

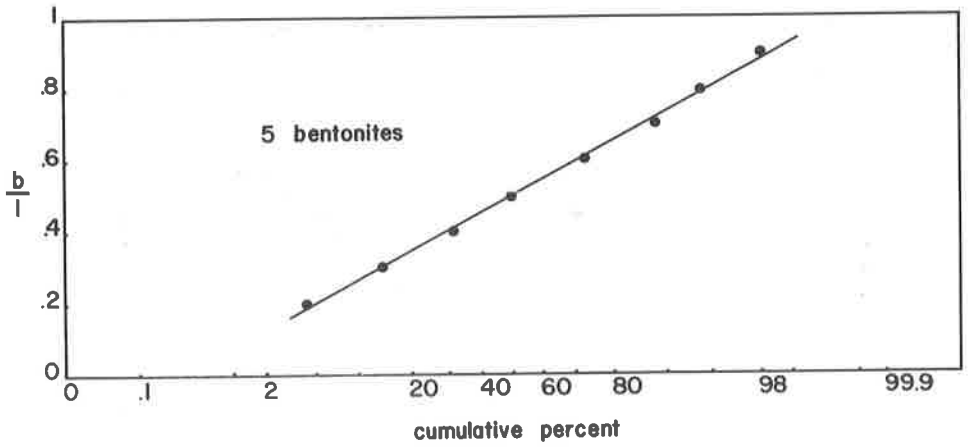

Figure 4. Plot of elongation ratio (b/l) for the five bentonites vs. cumulative percent on arithmetic probability paper.

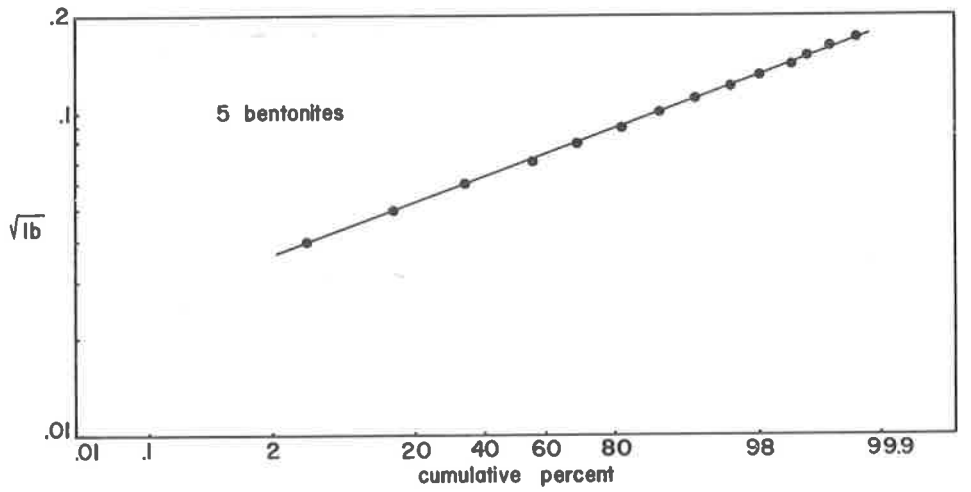

Figure 5. Plot of size ($\sqrt{lb}$) for the five bentonites vs. cumulative percent on log probability paper.

that the size data ($\sqrt{lb}$) are lognormally distributed. In the case of the elongation ratio there is, for all practical purposes, a lower limiting value of approximately 0.1 and an upper limiting value of 1.0. When the mode of the distribution falls close to the lower limiting value, which is true of the size data, the sample is positively skewed and approximates the lognormal distribution seen in Figure 5. A plot of the volume data will also yield a lognormal distribution. As $\sqrt{lb}$ is dimensionally a linear measure, it should be lognormal for growth in a homogeneous medium. Thus the zircon suites probably represent a homogeneous population with respect to size. If the mode is centrally

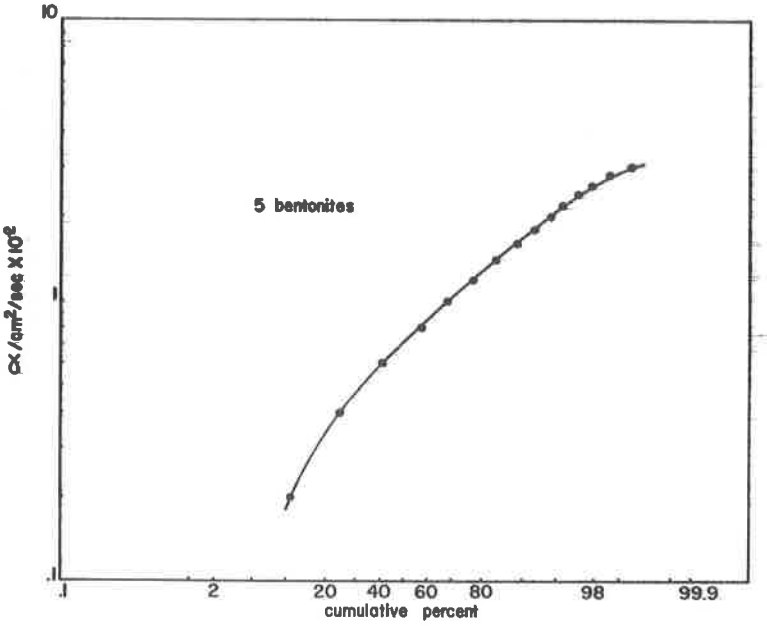

Figure 6. Plot of α-activity for the five bentonites vs. cumulative percent on log probability paper.

disposed between the lower and upper limiting values, as it is in the case of the elongation ratio data, a normal distribution will result (Figure 4). It follows that if the mode is near the upper limiting value, the sample will be negatively skewed. These relationships have been discussed in more detail in connection with the distribution of trace and major elements in rocks by Rogers and Adams (1963). In any case, the data suggest that the bentonite zircon samples were drawn from a homogeneous population, all zircons crystallizing under similar physicochemical conditions. Similar plots of size and elongation ratio from the other samples do not yield straight lines.

The cumulative frequency distribution for the α-activity of bentonite zircons (Figure 6) does not plot as a straight line on log probability or probability paper and requires a special explanation. One explanation could be that the distribution is bi- or multimodal, but this is probably not the case, as evidenced by the histograms in Figure 1. These histograms show that the data are positively skewed, but not sufficiently for a lognormal distribution. Thus the mode must be between the "centrally disposed" value and the lower limiting value, suggesting the fact that despite the lack of normality, the sample was drawn from a homogeneous population, with respect to α-activity. Ahrens (1965) found that uranium and thorium distributions in zircons from granitic rocks approximate lognormality.

During the coarse of the study, it became necessary to quantify the degree of rounding and transparency of the zircon crystal. This was done by calculating a "rounding ratio" and "transparency ratio" for each suite. The rounding ratio is defined as the number of euhedral and subhedral crystals divided by the number of well-rounded crystals; the transparency ratio is defined as the number of transparent and translucent crystals divided by the number of "frosted" crystals. Note that the term opaque is avoided. Zircons that are described in the literature as opaque are referred to as malacons or are metamict. Metamict zircons and malacons are also highly radioactive compared to "ordinary" zircons, which is not the case with the frosted zircons. These frosted zircons are opaque or near-opaque, but this may be accounted for by the diffusion of light from the frosted surface. Observed with an oil immersion objective (total magnification, X1000), the surface of these frosted crystals appear to be pitted and abraded or possibly etched and corroded. Moreover, the euhedral crystals are generally transparent; subhedral crystals are commonly translucent; and rounded crystals are generally near-opaque. Metamict zircons and malacons were rarely observed and will be discussed later in this paper, but were not included in the calculation of rounding and transparency ratios.

Figure 7 is a plot of rounding ratio vs. transparency ratio for the zircon suites and, as expected, a positive correlation is evident. Note that the values for the bentonites and granite suites fall above those for the beach sand and two of the metamorphic suites. The zircons of the beach sand and two metamorphic rocks are in general highly rounded and abraded. They show evidence of considerable sedimentary recycling and reworking. Zircons from sample PCR-25C are the most euhedral, which suggests that this gneiss may be of igneous origin. This interpretation is in keeping with the field relationships for the rock from which PCR-25C was collected (Boyer and Clabaugh, 1959). Of the two indices, the rounding index seems best to characterize the suites, a value of greater than 1.0 indicating an igneous origin.

RADIOACTIVE SITES

Differences in electronegativities and size would indicate that U^{4+} and Th^{4+} have restricted entry into the Zr^{4+} lattice sites in zircons (Table 3). Both ions are roughly 20 percent larger than Zr^{4+} and can be much more easily accommodated in Y^{4+} or Ce^{4+} sites in xenotime or monazite, as evidenced by relatively high concentrations of both U and Th in monazite and xenotime compared with zircon (Hurley and Fairbairn, 1957).

Electronegativity values for both U^{4+} and Th^{4+} are the same and are quite similar to that for Zr^{4+}. Reliable ionization potential data for U^{4+} and Th^{4+} are not available, but Taylor (1965) points out that the melting point of ThO_2 is 3050°C as compared to 2176°C for UO_2,

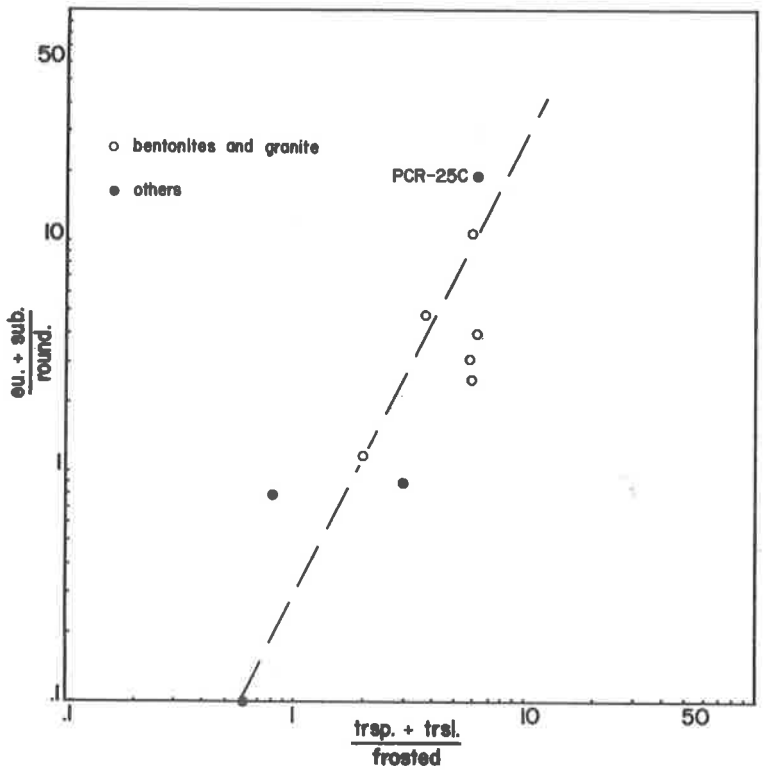

Figure 7. Plot of rounding ratio (euhedral + subhedral grains / rounded grains) vs. transparency ratio (transparent + translucent grains / frosted grains).

Table 3. Ionic radii and electronegativities for zirconium and some related elements.

	r*	e**
Zr^{4+}	0.79	1.5
Hf^{4+}	0.78	1.4
Th^{4+}	1.02	1.4
U^{4+}	0.97	1.4
Y^{4+}	0.92	1.2
Ce^{4+}	0.94	1.1

*in angstroms; data taken from Ahrens (1952).
**electronegativity values from Gordy and Thomas (1956).

which suggests that the Th-O bond is considerably more ionic than the U-O bond. Thus if one takes into account relative bond types, the average Th/U ratio in zircons of a magmatic series should decrease with differentiation. On the other hand, Ahrens (1965) has suggested that U^{4+} may be preferentially accepted because its ionic radius is closer to that of Zr^{4+}. He cites as evidence the fact that the Th/U ratio is generally much smaller in the zircons than in their host rocks. This reasoning would imply that the Th/U ratio might be higher in zircons from more fractionated igneous rocks. The average Th/U ratio for zircons from granites as reported in Hurley and Fairbairn (1957) is 0.4, whereas the ratio for pegmatitic zircons is 1.0. Assuming that pegmatites are generally late-stage fractionates of granites, it would seem that small differences in ionic size control the preferential entry of U^{4+}, rather than differences in bonding.

The above arguments hold only if Th^{4+} and U^{4+} are competing for lattice sites in the zircons. The fact that at least limited substitution does exist is indicated by the data in Table 4, showing the distribution of radioactivity within the zircon suites. In every case over 90 percent of the α-tracks were observed to project randomly from the crystals. The α-track density over the crystals was quite uniform. Only in sample PCR-65 were an appreciable number (10.2 percent) emitting from surface coatings and the inclusions were no more radioactive than the surrounding zircon crystals. Silver and Deutsch (1963) made similar observations when they found that little of the α-activity seems to be localized in an individual zircon crystal. It would appear, therefore, that despite their relatively large ionic radii, U^{4+} and Th^{4+} can substitute for Zr^{4+} in crystal lattices. No local concentrations of α-activity were seen within a single crystal, suggesting that occlusion did not take place to an appreciable degree.

Another explanation of the higher Th/U ratios in zircons from pegmatites involves the oxidation of U^{4+} to its more soluble form $(UO_2)^{2+}$ and its subsequent leaching from the crystal lattice. Such a process may take place owing to oxidative processes believed to be operative during the pegmatitic stage of magmatism (Rogers and Ragland, 1961; Ragland et al., 1967). Thus the relatively high Th/U ratios in pegmatitic zircons compared with granitic zircons may be caused by removal of U during the pegmatitic stage. This U eventually may find its way into secondary minerals or readily leachable material along grain boundaries.

One interesting observation made during the course of the study was that in several samples a relatively few highly radioactive grains accounted for a disproportionally large amount of the α-activity. Silver and Deutsch (1963) also noted this when they found that less than one percent uranothorite grains in a zircon suite from the Johnny Lyon Granodiorite, Arizona, can account for more than 50 percent of the radioactivity. The pertinent data are given in Table 4. For example, in sample PCR-1 normal zircons accounted for 86 percent of the suite

Table 4. Distribution of Radioactivity Within the Zircons.

Sample	% distribution of ∝-activity within zircons: random	x'lline inclusions	opaque inclusions	opaque coatings	% total ∝-activity attributable to zircon*	% zircons* in suite
KIN-2	94.9	1.9	2.1	1.1	100	100
GH-12	100	---	---	---	100	100
JHT-8	92.6	1.4	1.6	4.4	78	99
GH-26	93.3	3.7	3.0	---	65	98
GH-14	100	---	---	---	100	100
LAU-1	99.4	---	0.6	---	27	79
PCR-65	89.6	---	0.2	10.2	75	96
PCR-25C	97.9	1.5	0.7	---	49	95
PCR-1	98.3	---	1.7	---	8	86
FBS-1	98.7	0.2	0.3	0.8	44	98

*excluding malacon and metamict zircons

but only 8 percent of the radioactivity.

Several possibilities exist as to the nature of these highly radioactive grains. A few of them (less than 10 percent) are apparently zircons. There are three known varieties of zircons, normal or high zircon, hyacinth and malacon or low zircon. Normal zircons are characterized by relatively low radioactivities, high indices of refraction, high birefringences and high specific gravities. They are generally colorless, transparent and euhedral. Malacons are characterized by relatively high radioactivities, low indices of refraction, low birefringences and low specific gravities. They are commonly brown to black in color, translucent to opaque and rounded. Hyacinths are intermediate between the other two varieties of zircons in every respect and are generally pink to purple in color. See Hutton (1950) and Morgan and Auer (1941) for a detailed discussion of the three varieties of zircons. In addition, metamict zircons, those whose crystalline lattices have been destroyed by radiation damage and are now isotropic, are very highly radioactive. Hyacinths, malacons or metamict zircons are not observed in the bentonite suites. A few of the highly radioactive grains in sample PCR-1 are apparently malacons and metamict zircons.

The majority of the highly radioactive grains were not zircons but monazite, which was not separated from the zircons with the magnetic separator and heavy liquids. The identification was confirmed by mounting individual grains in an x-ray diffraction powder camera, exposing the film for 12-24 hours, and identifying the spots on the developed film. Approximately 20 grains were picked randomly and individually analyzed from several suites, and in each case the crystal was identified as monazite.

CRYSTAL HABIT

Hutton (1951) reports that the most common crystal habit for zircon is the development of second-order prisms a(110) terminated by first-order pyramids p(111), with or without third-order pyramidal faces. The prism m(110) was reported generally to be present but was rarely dominant. Less common are the development of second-order prisms with three orders of pyramids. The most simple habit of one prism and a pyramid of the same order, i. e., p(101) a(100) is reportedly uncommon.

The crystal habits of zircons observed in this study can be divided into three general groups, based upon their relative complexities. In order of their increasing complexity, typical examples of each group are: Type I, p(101) a(100); Type II, p(101) m(110) a(100); and Type III, p(101) m(110) a(100) x(211). These examples are illustrated in Figure 8. The drawings were taken from Berry and Mason (1959). Relative percentages of each type are given in Table 5 for those suites that contained an appreciably number of euhedral crystals.

With the exception of JHT-8 and PCR-25C, the simple habit of Type I is uncommon, which is in agreement with the observations of Hutton (1951). The most complex habit of Type III predominates. The data for LAU-1 are in good agreement with the conclusions of Hoppe (1965) concerning crystal morphology of the zircons from the Lausitz Granodiorite.

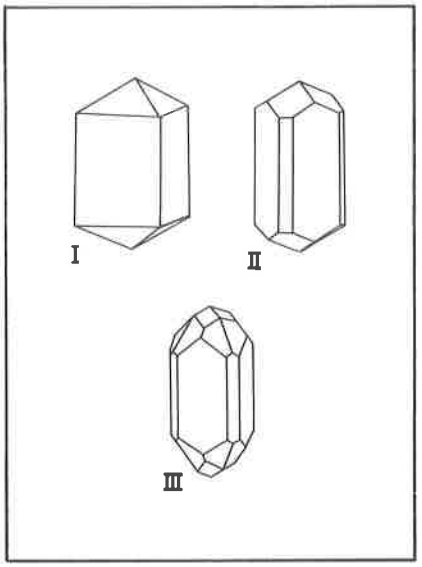

Figure 8. Typical examples of zircon crystals from Types I, II, and III. Drawings from Berry and Mason (1959).

Table 5. Relative Percentages of the Three Types of Crystals.

Sample	I	II	III
GH-12	0	19	81
GH-14	4	17	79
JHT-8	21	58	21
GH-26	8	27	65
KIN-2	5	45	50
PCR-25C	26	63	11
LAU-1	0	32	68

Table 6. Means and Standard Deviations of Volumes From Crystals of Types II and III.

	vol. $x10^{-4}$ mm^3 = $1xb^2$	
	Type II $\bar{x} \pm s$	Type III $\bar{x} \pm s$
PCR-25C	5.4 ± 1.6	2.2 ± 0.9
GH-12	4.3 ± 3.0	2.2 ± 1.2
GH-14	7.2 ± 6.0	5.0 ± 4.4
JHT-8	2.7 ± 1.7	1.7 ± 1.0
LAU-1	1.5 ± 1.2	1.1 ± 1.0
KIN-2	1.5 ± 0.9	1.2 ± 0.6
GH-26	5.3 ± 4.3	4.5 ± 3.6

During the course of the research it became apparent that there is a relationship between crystal habit and size of the crystals. The pertinent data are given in Table 6, which compares average volumes of Type II and Type III crystal habits for seven suites. Although the standard deviations are large in most cases, the arithmetic means are invariably larger for Type II crystals. Application of Student's t-test indicates a significant difference of means for zircons of all suites at the 99 percent confidence level.

The explanation for this observation may be found in an alternative expression of the well-known law of Bravais: "The rate of crystal growth in any lattice direction is proportional to the point density in that direction" (Berry and Mason, 1959, p. 48). The greatest point density will be in lattice planes with lowest Miller indices and crystal growth will be most rapid in those directions. Thus as a crystal grows, crystal faces with high Miller indices will tend to disappear and faces with low Miller indices will tend to enlarge. One would expect, therefore, crystals of Type III, containing some faces with relatively high Miller indices, to be smaller than crystals of Type II. This relation-

ship is in agreement with the data in Table 6. Those of Type I should be largest of all but insufficient data are available for all but one suite. In sample PCR-25C the average volume of Type I crystals is 5.4 $\pm$ 3.0 $mm^3 \times 10^{-4}$, equal to that of Type II.

CONCLUSIONS

1. Parameters that apparently best characterize a zircon suite and enable it to be distinguished from other suites are elongation ratio, rounding ratio and dispersion of volume histograms.

2. Zircons from the five bentonites are apparently from a homogeneous population with respect to size, elongation and α-activity, indicating that they crystallized under similar physicochemical conditions.

3. Apparently U^{4+} and Th^{4+} occupy regular lattice positions in zircon.

4. Relatively high Th/U ratios in pegmatitic zircons compared with granitic zircons may be explained by: (1) preferential entry of U^{4+} into the zircon lattice during magmatic fractionation; and (2) oxidation of U^{4+} to $(UO_2)^{2+}$ and its subsequent leaching during the pegmatitic stage of magmatism.

5. A few grains in some of the suites that were observed to be considerably more radioactive than normal zircons are generally monazite and rarely malacon or metamict zircons.

6. Zircons with relatively complex crystal habits (i.e., they have some faces with comparatively high Miller indices) are in general smaller than those with less complex crystal habits. This observation can be explained by an alternative expression of the law of Bravais.

REFERENCES CITED

Adams, J. A. S., Edwards, G., Henle, W. K., and Osmond, J. K., 1960, Further progress in absolute dating of the Middle Ordovician: Nature, v. 188, p. 636-638.

Adams, J. A. S., and Rogers, J. J. W., 1961, Bentonites as absolute time-stratigraphic calibration points: in Geochronology of rock systems, N. Y. Acad. Sci. Annals, v. 91, p. 340-344.

Ahrens, L. H., 1952, The use of ionization potentials: Part I ionic radii of elements, Geochim. et Cosmochim. Acta, v. 2, p. 155-169.

_____, 1965, Some observations on the uranium and thorium distributions in accessory zircon from granitic rocks: Geochim. et Cosmochim. Acta, v. 29, p. 711-716.

Alper, A. M., and Poldervaart, A., 1957, Zircons from the Animas stock and associated rocks, New Mexico: Econ. Geol., v. 52, p. 952-971.

Berry, L. G., and Mason, B., 1959, Mineralogy: W. H. Freeman and Co., San Francisco, 629 p.

Boyer, R. E., and Calbaugh, S. E., 1959, Geology of the Red Mountain Gneiss, Llano County, Texas: Bull. Geol. Soc. Am., v. 70, p. 1572.

Byström-Asklund, A. M., Baadsgaard, H., and Folinsbee, R. L., 1961, K/Ar age of biotite, sanidine, and illite from Middle Ordovician bentonites at Kinnekulle, Sweden: Geol. Fören Stockh. Förh., v. 83, p. 92-96.

Eckelmann, F. D., and Kulp, J. L., 1956, Sedimentary origin of the Cranberry and Henderson "granites" in North Carolina: Am. J. Sci., v. 254, p. 316-324.

Gordy, W., and Thomas, W. J. O., 1956, Electronegativities of the elements: J. Chem. Phys., v. 24, p. 439-444.

Hammill, G., 1957, The radioactivity, accessory minerals, and possibilities for absolute dating of bentonites: M. A. Thesis, Rice University.

Hoppe, G., 1965, Morphologische Unterschungen als Beiträge zu Zirkon-Alters Bestimmungen: N. Jb. Miner., v. 103, p. 273-285.

Hurley, P. M., and Fairbairn, H. W., 1957, Abundance and distribution of uranium and thorium in zircon, sphene, apatite, epidote, and monazite in granitic rocks: Trans. Am. Geophys. Union, v. 38, p. 939-944.

Hutton, C. O., 1950, Studies of heavy detrital minerals: Bull. Geol. Soc. Amer., v. 61, p. 635-710.

Imbrie, J., 1956, Biometrical methods in the study of invertebrate fossils: Am. Mus. Nat. Hist. Bull, v. 108, p. 215-252.

Jaffe, H. W., Gottfriend, D., Waring, C. L., and Worthing, H. W., 1959, Lead-alpha age determinations of accessory minerals of igneous rocks: U. S. Geol. Survey Bull. 1097, p. 65-148.

Larsen, L. H., and Poldervaart, A., 1957, Measurement and distribution of zircons in some granitic rocks of magmatic origin: Mineral Mag., v. 31, p. 544-564.

McIntire, W. L., 1963, Trace element partition coefficients--a review of theory and applications to geology: Geochim. et Cosmochim. Acta, v. 27, p. 1209-1264.

Morgan, J. H. and Auer, M. L., 1941, Optical, spectrographic and radioactivity studies of zircon: Am. J. Sci., v. 239, p. 305-311.

Poldervaart, A., 1955, Zircon in rocks, I. Sedimentary rocks: Am. J. Sci., v. 253, p. 433-461.

_____, 1956, Zircon in rocks, II. Igneous rocks: Am. J. Sci., v. 254, p. 521-554.

Poldervaart, A., and Eckelmann, F. D., 1955, Growth phenomenon in zircon of autochthonous granites: Bull. Geol. Soc. Am., v. 66, p. 947.

Ragland, P. C., 1961, Geochemical and petrological studies of the

Lost Creek Gneiss, Mason and McCulloch Counties, Texas: M. A. Thesis, Rice University.

Ragland, P. C., 1964, Autoradiographic investigations of naturally occurring materials: in The Natural Radiation Environment, (Eds. Adams and Lowder), p. 129-151.

Ragland, P. C., Billings, G. K., and Adams, J. A. S., 1967, Chemical fractionation and its relationship to the distribution of thorium and uranium in a zoned granitic batholith: Geochim. et Cosmochim. Acta, v. 31, p. 17-34.

Rogers, J. J. W., and Adams, J. A. S., 1963, Lognormality of thorium concentrations in the Conway granite: Geochim. et Cosmochim. Acta, v. 27, p. 775-784.

Rogers, J. J. W., and Ragland, P. C., 1961, Variation of thorium and uranium in selected granitic rocks: Geochim. et Coschim. Acta, v. 25, p. 99-109.

Saxena, S. K., 1966, Evolution of zircons in sedimentary and metamorphic rocks: Sedimentology, v. 6, p. 1-33.

Schurmann, H. M. E., Bot, A. C. W. C., Steensma, J. J. S., Suringa, R., Eberhardt, P., Geiss, J., Vongunten, H. R., Houtermans, F. G., and Singer, P., 1956, Second preliminary note on age determinations of magmatic rocks by means of radio-activity: Geol. en. Mijnbouw, v. 18, p. 312-330.

Silver, L. T., and Deutsch, S., 1963, Uranium-lead isotopic variations in zircons: a case study: J. of Geol., v. 71, p. 721-758.

Taylor, S. R., 1965, The application of trace element data to problems in petrology: Phys. and Chem. of the Earth, v. 6, p. 133-214.

Terrell, J., 1960, Separation of zircon and biotite from bentonite and absolute dating possibilities for dating certain West Texas bentonites: M. A. Thesis, Rice University.

Wilson, C. W., Jr., 1949, Pre-Chattanooga stratigraphy in central Tennessee: Bull. Tenn. Dept. of Conserv., Div. of Geol., v. 56, 407 p.

GEOLOGY OF THE SOUTHWESTERN BALD MOUNTAINS IN THE BLUE RIDGE PROVINCE OF TENNESSEE

By

Denny N. Bearce
Department of Geology
Birmingham-Southern College
Birmingham, Alabama

ABSTRACT

The southwestern Bald Mountains in eastern Tennessee are part of the western margin of the Blue Ridge Province in the southern Appalachians.

Two major thrust sheets occur in the southwestern Bald Mountains: the Buffalo Mountain thrust sheet and the Del Rio thrust sheet. Both thrust sheets are composed largely of clastic sedimentary rocks of the Precambrian Ocoee Series and the Lower Cambrian Chilhowee Group.

Synclines in both the Buffalo Mountain and Del Rio thrust sheets indicate post-fault folding of the thrust sheets. Imbricate thrust faulting developed during the folding of the larger thrust sheets. A greater intensity of folding is expressed at the surface in the Del Rio thrust sheet than in the overlying Buffalo Mountain thrust sheet.

Small windows in the Del Rio thrust sheet indicate that the imbricate thrust faults within the sheet become subhorizontal at a relatively shallow depth and are folded. The Del Rio thrust sheet probably thins northeastward by wedging out from the base upward beneath the Buffalo Mountain thrust sheet. Possibly, only the lower portion of the Del Rio thrust sheet, the most deformed portion nearest the sole fault of the thrust sheet, remains; the upper portion may have been bevelled by the over-riding Buffalo Mountain thrust sheet and subsequently further reduced by erosion. Deformational intensity increases near the southwest end of the Buffalo Mountain thrust sheet where it wedges out over the Del Rio thrust sheet. The increased degree of deformation in the thinned southwest end of the Buffalo Mountain thrust sheet and the even greater deformation in the northeasternmost exposed portion of the Del Rio thrust sheet suggest that the northeastern exposed portion of the Del Rio thrust sheet is a surface representation of the structural nature of the Buffalo Mountain thrust sheet at depth.

A more or less continuous synclinal trend with minor intervening warps is postulated to extend from the synclinorium, between the Holston Mountain and Iron Mountain thrust faults of northeasternmost

Tennessee, southwestward to the southwest end of the Buffalo Mountain thrust sheet where it is expressed by the Paint Creek and Greene Mountain synclines. The northeast-plunging nose of the Paint Creek syncline is reflected in the curved trace of the Buffalo Mountain thrust fault, which bounds both the southwest end of the Buffalo Mountain thrust sheet and the east side of the Hot Springs window in North Carolina to the southeast. Late stage folding of the Buffalo Mountain thrust sheet perpendicular to the direction of movement produced the synclines.

INTRODUCTION

The southwestern Bald Mountains of the Unaka Range form a portion of the western margin of the Blue Ridge Province in the Southern Appalachians (Figure 1). The Bald Mountains extend from the northeastern end of the Great Smoky Mountains northeastward about 50 miles along the Tennessee-North Carolina border. The southwestern Bald Mountains considered here (Figure 1) extend from Lanceville, Cocke County, Tennessee, northeastward through Greene County, Tennessee, to Big Butt Mountain, Tennessee, an area roughly 21 miles long and 3 miles wide (Plate 1).

Exposed rocks in the southwestern Bald Mountains belong mainly to the Ocoee Series and Chilhowee Group (Safford 1869, pp. 113-203) of late Precambrian and early Cambrian age respectively. The sequence consists of shale, siltstone, sandstone and conglomerate and includes minor intervals of dolomite and limestone. Although basalt flows are present in the Chilhowee Group immediately northeast, no igneous rocks have been observed in the southwestern Bald Mountains. The sedimentary rocks have in part been metamorphosed to quartzite and slate.

Rocks within the Bald Mountains have been thrust northwestward over Ordovician limestone and shale of the Valley and Ridge Province along the Holston Mountain, Buffalo Mountain, and Meadow Creek Mountain thrust faults (Figure 2). In the southwestern Bald Mountains two major thrust sheets are recognized: the Buffalo Mountain thrust sheet, bounded by the Buffalo Mountain thrust fault; and the Del Rio thrust sheet, bounded by the Meadow Creek Mountain thrust fault (Figure 2). The Del Rio thrust sheet underlies the Buffalo Mountain thrust sheet. Minor thrust faults within both thrust sheets cause numerous gaps and repetitions in the stratigraphic column.

Acknowledgments

The writer is grateful for the financial assistance received from the Tennessee Division of Geology and the National Science Foundation while mapping the southwestern Bald Mountains. He is indebted to G. D. Swingle, H. J. Klepser, and L. T. Larsen of the University of

KY.
VA.
ORDOVICIAN
CAMBRIAN
CHILHOWEE GROUP
PRECAMBRIAN
OCOEE SERIES

ern
rn.
ern

s a

sequence of clastic sedimentary rocks with minor intervals of limestone and dolomite, and with no known fossils. The Ocoee Series is of limited extent in the Unaka Mountains of eastern Tennessee, the western Carolinas, Georgia, and possibly Alabama. On the southeast side of the Unakas the Ocoee rests nonconformably on older granites and gneisses. In the northwestern portion of the Unakas the Ocoee is overlain conformably or paraconformably by the basal formation of the Chilhowee Group.

The Ocoee Series has been assigned a late Precambrian age (King, et al., 1958, p. 965) and has been classified by the U. S. Geological Survey as a provincial series (King, et al., 1958, p. 951), analogous to the Keweenawan, Beltian, Grand Canyon, and others.

Northeastward from the Great Smoky Mountains the Ocoee Series thins abruptly from its base upward; Ocoee sediments in the southwestern Bald Mountains are thought to correlate mainly with youngest Ocoee sediments, the Walden Creek Group, in the Smokies (King, 1949, p. 628).

A two-fold subdivision of the Ocoee Series into the Snowbird Formation and Sandsuck Formation, in ascending order, was used by the writer in mapping the southwestern Bald Mountains. These mapping units were chosen in preference to the units used in mapping portions of the Great Smoky Mountains (King, 1964) for two reasons. First, the primary purpose of the present investigation was to fill a gap between previously mapped areas in northeast and east Tennessee. In the previously mapped areas bordering the present area of investigation on the northeast (Shekarchi, 1959, p. 62-74) and on the southwest (Ferguson, 1951, p. 13-17) the Snowbird and Sandsuck Formations were used as mapping units. By using the same units the writer could more easily correlate, compare, and note stratigraphic trends between these adjoining areas. Secondly, such a two-fold division is logical in the southwestern Bald Mountains. The preponderance of feldspathic quartzite and arkose in the Snowbird, and the preponderance of slate and siltstone with lenses of dolomite and limestone in the Sandsuck, serve to differentiate the two formations in the area of investigation.

Snowbird Formation. The Snowbird Formation (Keith, 1904, p. 5) in the southwestern Bald Mountains consists of approximately 4,500 feet of greenish grey to light brown, massively-bedded arkose and light brown, medium- to massively-bedded, feldspathic quartzite with intervals of grey to black shale and slate (Figure 3). Quartzites and arkoses within the formation support knobs and ridges such as Big Butt, Black Stack Cliff, White Rock Cliff, Little Bald Mountain, Camp Creek Bald, and Rich Mountain (Plate 1).

The Snowbird Formation is overlain conformably by shale and siltstone of the Sandsuck Formation. The base of the Snowbird Formation is not exposed in the area shown in Plate 1.

Two facies of the Snowbird are found along strike in the southwestern Bald Mountains. The southwestern facies occupies the

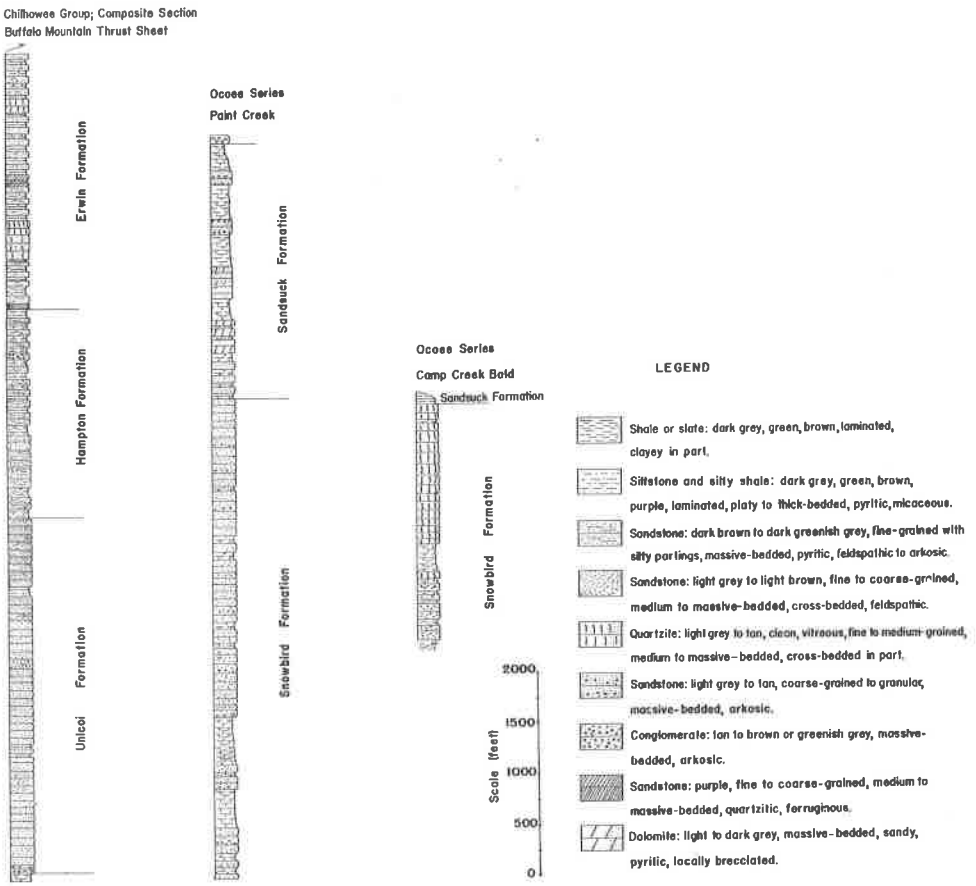

Figure 3. Columnar sections, Southwestern Bald Mountains, Tennessee.

southwest end of the Buffalo Mountain thrust sheet (Plate 1). The northeastern facies is found in a different thrust block within the Buffalo Mountain thrust sheet northeast of State Highway 70 (Plate 1). The northeastern facies is typified by units 50 to 1,000 feet thick of light brown to light grey, medium- to massively-bedded, vitreous in part, fine- to coarse-grained quartzite containing intervals of granular arkosic quartzite, and units approximately 300 feet thick of dark greenish-grey, massively-bedded, fine- to medium-grained, spheroidally weathering, arkosic sandstone containing intervals of platy to thin-bedded siltstone and shale (Figure 3, Ocoee Series, Camp Creek Bald). The southwestern facies is composed of pale greenish-grey and greenish-brown, massively-bedded (beds as much as 20 feet thick), fine- to coarse-grained arkose with intervals of conglomeratic arkose up to five feet thick, and grey to black, laminated shale and siltstone (Figure 3, Ocoee Series, Paint Creek). No distinctive lithology can be traced from one facies into the other, and thrust faulting prevents a comparison of thickness between the two facies (Figure 3).

Sandsuck Formation. The Sandsuck Formation (Keith, 1895, p. 3) in the southwestern Bald Mountains comprises 2,500 feet of dark-

green, dark- to light-grey, black, and dark-red pyritic shale and siltstone; light-brown to grey, coarse-grained to conglomeratic, thick-bedded arkose; and grey, sandy, thick-bedded, pyritic, dolomite (Figure 3). The shale and siltstone in part have been metamorphosed to slate. The Sandsuck Formation in the southwestern Bald Mountains is apparently overlain conformably by arkosic conglomerates of the Unicoi Formation.

Chilhowee Group

General. The Chilhowee Group (Safford, 1869, p. 198-203) (Keith, 1903, p. 4-5) is a sequence of clastic sedimentary rocks of variable thickness, equivalents of which are found in the Blue Ridge Province from Pennsylvania to Georgia. A three-fold subdivision of the Chilhowee Group (Keith, 1903) is used in northeastern Tennessee including the southwestern Bald Mountains, but a five-fold subdivision (Keith, 1905) is used in the Great Smoky Mountains to the southwest (Table 1). The occurrence of Indiana tennesseensis in the Murray Slate (Laurence and Palmer, 1963, p. 53-54) and of Scolithus linearis in beds as low as the Unicoi Formation (King et al., 1944, p. 29) have caused the Chilhowee Group to be assigned to the Cambrian.

Table 1. Correlation of Chilhowee Group on Chilhowee Mountain with Northeastern Equivalents as Proposed by King (1964, p. 71).

Chilhowee Mountain	Northeastern Equivalents
Hesse Quartzite)	
)	
Murray Slate)	Erwin Formation
)	
Nebo Quartzite)	
Nicols Slate	Hampton Formation
Cochran Conglomerate	Unicoi Formation

The Chilhowee Group of the southwestern Bald Mountains changes in character upward from coarse-grained arkose in the Unicoi to clean, fine-grained quartzites and siltstones in the Erwin. It appears that with passage of time the provenance area for Chilhowee sediment either shifted or was reduced to low relief.

Unicoi Formation. The Unicoi Formation (Keith, 1903, p. 4-5) of the southwestern Bald Mountains consists of about 3,000 feet of light-grey, medium- to thick-bedded, medium- to coarse-grained, feldspathic

quartzite and arkose, brown to greenish-grey, medium- to thick-bedded, fine-grained, pyritic sandstone, and minor intervals of dark-grey, platy siltstone (Figure 3). The lower half of the formation becomes increasingly more arkosic and granular toward the base, and generally ten to seventy feet of arkosic conglomerate with white quartz and yellow feldspar pebbles forms the lowermost beds of the formation.

The Unicoi is overlain conformably by shale and siltstone of the Hampton Formation. It is distinguished from the underlying Sandsuck Formation by the preponderance of shale and siltstone, and by the occurrence of dolomite beds or dolomite cement in arkosic intervals, within the Sandsuck.

Hampton Formation. The Hampton Formation (Keith, 1903, p. 5) in the southwestern Bald Mountains is composed of about 2,000 feet of shale, siltstone, and sandstone (Figure 3). The sandstone is mainly dark-brown to grey, as are the shale and siltstone which form the major portion of the formation. Typical Hampton sandstone is fine-grained, massively-bedded and pyritic, and weathers to smooth, rounded ledges. Intervals of arkose and feldspathic quartzite similar to Unicoi lithology are present in the Hampton, but they constitute only a small percentage of the formation. The shale and siltstone of the Hampton are identical to the shale and siltstone in the major portion of the Erwin Formation. However, the Hampton contains no ferruginous quartzite or tan vitreous quartzite, the two lithologies which are distinctive of the Erwin in the southwestern Bald Mountains. Thus, the Hampton Formation is best delimited locally in terms of the more distinctive beds of the Unicoi and Erwin formations below and above it.

The Hampton Formation has essentially the same lithologic character in both the Buffalo Mountain and Del Rio thrust sheets. In the Del Rio sheet, however, a laterally presistent interval of feldspathic quartzite is present in the middle portion of the formation and is mapped as the Hampton Quartzite Member (Plate 1). The lower Hampton, present and used as a mapping unit (Ferguson, 1951, p. 28) in other portions of the Del Rio thrust sheet, is not exposed in the portion of the Del Rio thrust sheet mapped by the writer.

Erwin Formation. The Erwin Formation (Keith, 1903, p. 5) in the southwestern Bald Mountains is a 2,500 foot thick sequence of bluish-grey, finely-laminated siltstone and shale and light-gray, thin-bedded, fine-grained, pyritic sandstone with distinctive intervals of dark-red, medium- to massively-bedded, fine- to coarse-grained, ferruginous quartzite and light-brown, vitreous, massively-bedded quartzite (Figure 3). The latter two lithologies serve to differentiate the Erwin from the Hampton. The writer has mapped the base of the Erwin as the base of the lowest ferruginous quartzite in the southwestern Bald Mountains.

TECTONICS

Principal Structural Features of the Unaka Range in Northeastern Tennessee and Western North Carolina

Major thrust sheets. The dominant structural features of the Unaka Range are thrust faults which dip generally 30 degrees to 40 degrees toward the southeast. Because of shallow dip and great topographic relief the faults are commonly sinuous in trace and form branching or anastomosing patterns. The thrust planes generally cut across stratigraphic horizons at low angles.

The Holston Mountain thrust fault (Stose and Stose, 1944, p. 380) may be traced along the front of the Unaka Range for tens of miles in northeast Tennessee (Figure 2). It is a low-angle, southeast-dipping fault along which Precambrian and lower Cambrian rocks have moved relatively northwest over Ordovician rocks of the Valley and Ridge Province. The Holston Mountain fault is replaced southwestward as the boundary of the Blue Ridge Province, by the Buffalo Mountain fault which in turn is replaced further southwest by the Meadow Creek Mountain fault (Figure 2).

The Buffalo Mountain overthrust (Keith, 1907, p. 8-9) in the northeast part of the Bald Mountains bounds a tongue-shaped body of rocks called the Buffalo Mountain thrust sheet (Figure 2) Ordway, 1959, p. 623). The overthrust dips gently to the southeast on the northwest side and almost vertically on the southeast side of the thrust sheet (Rodgers, 1953, p. 142). On the southeast side of the tongue the Buffalo Mountain fault trace merges with the Rector Branch fault and for a small distance borders the southwest end of the Mountain City window (Figure 2). The Buffalo Mountain thrust fault forms the northwest boundary of the Bald Mountains as far southwest as Hayesville (Plate 1), where it arches back into the mountains.

At Hayesville the Buffalo Mountain fault is replaced as the west boundary fault of the Blue Ridge Province by the Meadow Creek Mountain thrust fault. The Meadow Creek Mountain and Mine Ridge thrust faults (Figure 2) delimit the Del Rio thrust sheet (Ferguson and Jewell, 1951, p. 40-44). The two faults may be separate exposures of a single folded fault. The Del Rio thrust sheet is cut into blocks by lesser, apparently steeper thrust faults, and contains the same formations as the Buffalo Mountain thrust sheet which overlies it. The Del Rio thrust sheet is in part overridden by the Buffalo Mountain thrust sheet and probably wedges out northeastward beneath the Buffalo Mountain thrust sheet.

Folds. King et al. (1944, p. 11), in describing the geology of northeast Tennessee, believed that thrust sheets had moved many miles northwest along low-angle thrust faults. He postulated that during or shortly after thrusting the thrust sheets were folded broadly into a

synclinorium to the northwest, between the Holston Mountain and Iron Mountain thrust faults, and an anticlinorium to the southeast, between the Iron Mountain and Stone Mountain thrust faults (Figure 2). King et al. (1944, p. 12) reported that the highest and youngest thrust sheet of the series of thrust sheets in northeastern Tennessee, the Buffalo Mountain thrust sheet, lies within the trend of the synclinorium (Figure 2).

The Rich Mountain syncline (Shekarchi, 1959) lies in the same trend as the synclinorium described by King between the Holston Mountain and Iron Mountain thrust faults (Figure 2). The smaller Greene Mountain and Paint Creek synclines southwest of the Rich Mountain syncline lie in the same trend as the Rich Mountain syncline. Thus, King's synclinorium appears to extend southwestward from northeasternmost Tennessee to the southwest end of the Buffalo Mountain thrust sheet.

Windows. The great horizontal displacement of thrust sheets of the Blue Ridge province is proven by windows that lie as much as 12 miles southeast of the edge of the thrust sheets.

The Mountain City window lies on the anticlinorium trend between the Iron Mountain and Stone Mountain thrust faults (Figure 2). The window exposes Precambrian granites and gneisses and lower Cambrian sedimentary rocks of the Chilhowee Group, Shady Formation and Rome Formation. Rocks within the window are cut by many thrusts dipping both southeast and northwest.

The Hot Springs window is encompassed by four different thrust faults. Rocks within the window range in age from the Cambrian Shady Formation to the Precambrian Snowbird Formation. The window trends east-west in contrast to the northeast alignment of most Appalachian structures (Figure 2). Oriel (1949, p. 156) reported a southwest-plunging anticline within the window. He proposed that the anticline formed within and after emplacement of an early thrust sheet, the Pulaski thrust sheet, which underlies the Buffalo Mountain and Del Rio thrust sheets.

Structural Features of the Buffalo Mountain and Del Rio Thrust Sheets Within the Southwestern Bald Mountains

Thrust faults. The Buffalo Mountain thrust fault is a low-angle fault dipping at the surface from 4 to 35 degrees to the southeast and flattening at depth (Figure 4). Stratigraphic relationships between hanging wall and footwall vary along the Buffalo Mountain thrust fault. The Snowbird rests on Cambrian Shady Dolomite at the southwest end of the thrust sheet and the Sandsuck and Unicoi rest on Ordovician Sevier Shale and Knox Limestone at the northeast end of the area of study. Never the less, stratigraphic displacement appears to be consistently of a magnitude of about 10,000 feet along the length of the fault. The

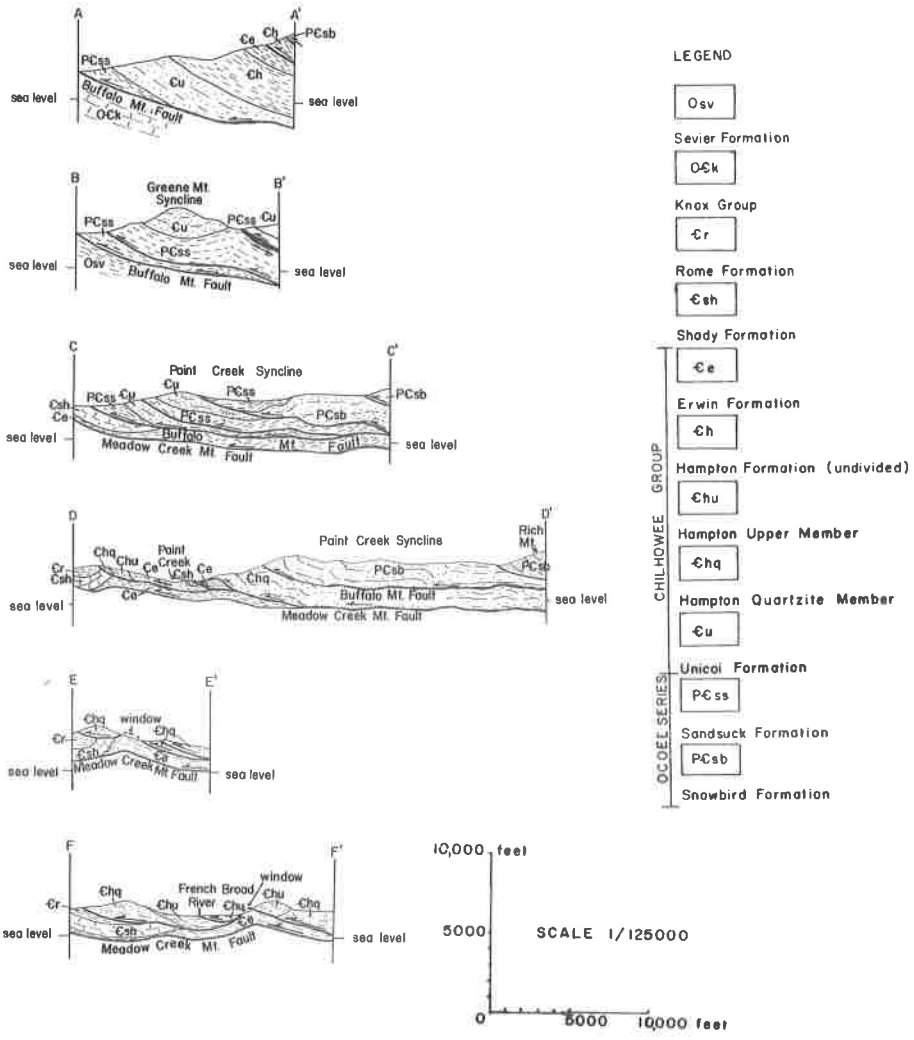

Figure 4. Structural cross sections of the southwestern Bald Mountains, Tennessee. Cross section lines are shown on Plate 1.

best evidence for the magnitude of horizontal movement along the Buffalo Mountain thrust fault is provided by the Hot Springs window. The minimum magnitude of horizontal movement, from the northwest border of the Buffalo Mountain thrust sheet to the southeast side of the Hot Springs window, is about 10 miles.

The Buffalo Mountain thrust fault cuts across beds in the Buffalo Mountain thrust sheet because bedding consistently dips more steeply than the fault (Figure 4, Sec. A-A'). The fault cuts successively older hangingwall strata toward the northwest margin of the thrust sheet and

southwestward along the trace of the fault.

The Del Rio thrust sheet, bounded by the Meadow Creek Mountain thrust fault, protrudes from beneath the Buffalo Mountain thrust sheet at its southwest end. Arkose of the Sandsuck Formation at the southwest end of the Buffalo Mountain thrust sheet is faulted onto a thin wedge of Shady Dolomite which in turn is carried by the Meadow Creek Mountain fault onto Sevier Shale of the Pulaski thrust sheet (Plate 1). Northeast from Hayesville, Sandsuck beds of the Buffalo Mountain thrust sheet lie directly on Sevier Shale of the Pulaski thrust sheet (Plate 1). The intermediate thin wedge of Shady Dolomite marks the northeasternmost exposure of the Del Rio thrust sheet that probably wedges out from its base upward beneath the Buffalo Mountain thrust sheet (Figure 5). The Buffalo Mountain thrust fault, replaced at the mountain front at Hayesville by the Meadow Creek Mountain thrust fault, assumes a more south-southwesterly course into the mountains across the Del Rio thrust sheet (Plate 1) and continues into North Carolina.

Numerous lesser thrust faults are found within the Buffalo Mountain and Del Rio thrust sheets. At the surface the lesser faults of the Buffalo Mountain thrust sheet generally dip about 45 degrees to the southeast (Figure 4). Thrust faults within the Del Rio thrust sheet are much more sinuous in trace than are those within the Buffalo Mountain thrust sheet, probably because the fault planes within the Del Rio thrust sheet do not dip so steeply as those within the Buffalo Mountain thrust sheet. Instead, fault planes within the Del Rio thrust sheet appear to form undulating surfaces at relatively shallow depth (Figure 4, Sections E-E' and F-F').

Stratigraphic displacement ranges to a maximum of about 3,500 feet for all but the southeasternmost fault of the Buffalo Mountain thrust sheet, slightly northwest of and roughly parallel to the Tennessee-North Carolina state line (Plate 1). Along the southeasternmost thrust fault of the Buffalo Mountain thrust sheet, quartzites and shales of the Snowbird Formation are faulted onto rocks as young as the Erwin Formation. The fault may be another imbricate thrust within the Buffalo Mountain thrust sheet; however, lack of resemblance of rocks in the hangingwall of the southeasternmost thrust fault to rocks elsewhere within the Buffalo Mountain thrust sheet may indicate that this is a separate major thrust sheet, higher and later than the Buffalo Mountain thrust sheet.

Synclines. The southwest nose of a northeast-plunging syncline, referred to herein as the Greene Mountain syncline (Bearce, 1966) occurs in the Buffalo Mountain thrust sheet (Plate 1 and Figure 4, Sec. B-B'). The northwest flank of the syncline, containing beds as young as the Erwin Formation, continues northeast beyond the northeast end of the area mapped by the writer. The southeast flank of the Greene Mountain syncline is concealed beneath higher thrust blocks from the upper Paint Creek headwaters northeastward (Plate 1). The southeast flank appears to project northeastward under the Rich Mountain syncline (Figure 2).

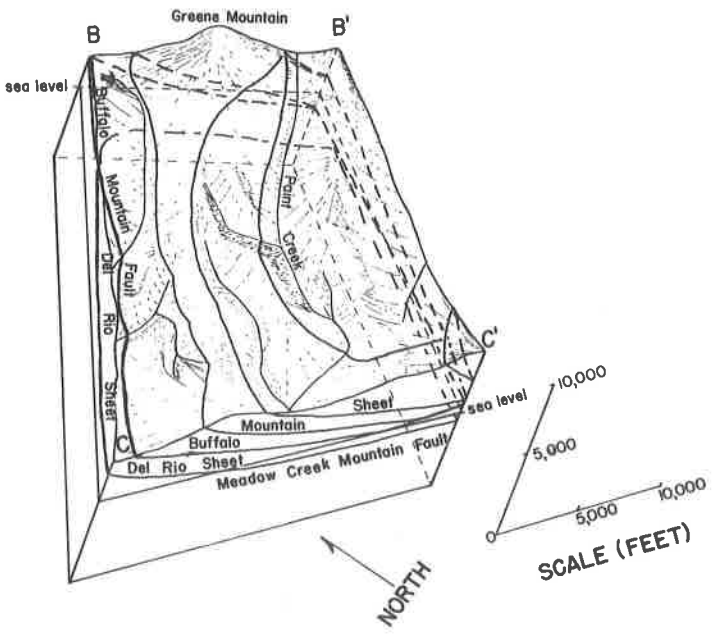

Figure 5. Block diagram between structure sections B-B' and C-C' showing northeastward wedge-out of Del Rio thrust sheet and southwestward thinning of Buffalo Mountain thrust sheet.

At the southwest end of the Buffalo Mountain thrust sheet is the northeast-plunging nose of the Paint Creek syncline (Bearce, 1966), a broad, faulted, and folded syncline containing beds at least as old as Snowbird and as young as the Unicoi Formation. One of the minor thrust faults in the Buffalo Mountain thrust sheet separates a large portion of the Paint Creek syncline from the Greene Mountain syncline.

The bedding attitude of the southwest nose of the Paint Creek syncline directly controls the map configuration of the eroded southwest end of the Buffalo Mountain thrust sheet; bedding strike is in part parallel to strike of the southwesternmost 2 miles of the Buffalo Mountain fault shown on Plate 1.

Minor shallow synclines within the Del Rio thrust sheet have axial trends that are inconsistent with the northeast trend of synclines in the Buffalo Mountain thrust sheet. Strata in the Del Rio thrust sheet are more intensely folded than strata of the Buffalo Mountain thrust sheet.

Windows. Two small windows, exposing rocks of the Erwin Formation and completely surrounded by quartzite and shale of the middle portion of the Hampton Formation, are found in the Del Rio thrust sheet in the lower Paint Creek-French Broad River area (Plate 1). The northernmost window, confined to the bottom of a deep stream

valley cut into Hampton beds, is approximately 3,200 feet long and is estimated to be 900 feet wide at its mid-point (Figure 4, Sec. E-E'). Rocks within the window consist of typical Erwin quartzites that dip 20 degrees to 35 degrees to the south. The second window lies on the south side of the French Broad River and is estimated to be about 450 feet in diameter. Rocks in the window are typical Erwin Formation, and the rocks surrounding the window are middle and upper Hampton (Figure 4, Sec. F-F'). Although exposures are few, the anomalous east dip of the quartzite within the window in contrast to the northwest dip of the surrounding Hampton beds, and the topographic location, at the bottom of a draw cut into Hampton beds, demonstrate a window.

Deformation within thrust blocks. In the portion of the Buffalo Mountain thrust sheet under consideration surficial deformation increases southwestward, reaching a maximum in the Paint Creek syncline. From the northeastern border of Plate 1 southwestward to the southwest nose of the Greene Mountain syncline, bedding attitudes reflect only broad warping of the blocks forming the Buffalo Mountain thrust sheet (Figure 4, Sections A-A' and B-B'). Southwest of the Greene Mountain syncline pronounced changes in degree of dip and reversals in direction of dip indicate more intense folding of the thrust blocks of the Buffalo Mountain thrust sheet (Figure 4, Sections C-C' and D-D').

Surficial evidence of increasing folding intensity southwestward in the Buffalo Mountain thrust sheet is accompanied by an increase in the development of fracture cleavage. Cleavage is absent northeast of the southwest nose of the Greene Mountain syncline. Cleavage is confined to Ocoee strata and reaches a maximum development in the Paint Creek syncline. The majority of cleavage attitudes have dips averaging from 50 to 75 degrees to the southeast and strikes averaging from N 10° E to N 30° E.

The thickness of strata overlying the Buffalo Mountain thrust fault in the Paint Creek syncline at the southwest end of the Buffalo Mountain thrust sheet is apparently less than it is further to the northeast in the thrust sheet. Southwestward thinning of the thrust sheet is due in part to erosion. Surface elevations along streams in the Buffalo Mountain thrust sheet from State Highway 70 northeastward are mostly above +2,000 feet; southwest of State Highway 70 they are generally between +1,500 feet and +2,000 feet (Plate 1). The Buffalo Mountain fault is conjectured to flatten at depth at an elevation between -1,000 feet and -2,000 feet (Figure 4, Sections A-A' and B-B') northeast of State Highway 70. The fault plane probably rises southwest of State Highway 70 over the northeast end of the Del Rio thrust sheet (Figure 4, Sections C-C' and D-D' and Figure 5). Thinning of the thrust sheet southwestward is thus mainly a result of wedging out above the Del Rio thrust sheet.

The intensity of folding is even greater in the northeasternmost

exposed portion of the Del Rio thrust sheet. Successively younger formations exposed northeastward at the toe of the Del Rio thrust sheet indicate that the sheet wedges from the base upward in a northeastward direction. Elevations along the traces of both the Meadow Creek Mountain fault and the Buffalo Mountain fault are between +1, 500 and +2, 000 feet (Plate 1); however, surface elevations along streams in the northeastern portion of the Del Rio thrust sheet are generally below +1, 500 feet (Plate 1). The northeastern end of the Del Rio thrust sheet was probably bevelled by the over-riding Buffalo Mountain thrust sheet. Subsequent erosion has caused the southwest end of the Buffalo Mountain thrust sheet to retreat eastward and has further thinned the Del Rio thrust sheet, producing windows on anticlinal folds within the thrust sheet.

The sum effect of the wedging of the two thrust sheets and of successively deeper erosion from Greene Mountain southwestward across the Paint Creek syncline to the northeastern portion of the Del Rio thrust sheet is to reveal the changes in structural nature that occur with depth in the major thrust sheets. The two small windows in the Del Rio thrust sheet provide an important clue to the structural nature and history of the thrust sheets forming and underlying the southwestern Bald Mountains. The windows indicate that the imbricate thrust planes within the major thrust sheets assume a sub-horizontal warped attitude at depth. Folding, both of imbricate thrust faults and of beds overlying them, is most intense near the planes of the major thrust faults. The folds project upward in the beds overlying each imbricate thrust fault, gradually attenuating and disappearing where the strata are thickest, as is the case northeast of the Paint Creek syncline in the Buffalo Mountain thrust sheet.

CONCLUSIONS

The controlling mechanism of the structure of the southwestern Bald Mountains is thrust faulting. Portions of two major thrust sheets, similar in stratigraphy but of contrasting structural character, are present in the southwestern Bald Mountains. The Del Rio thrust sheet is the older of the two thrust sheets and is overridden at its northeastern end by the Buffalo Mountain thrust sheet. Each thrust sheet moved into place, became folded and concurrently broken into smaller thrust blocks.

Although their structural histories are similar, the two thrust sheets differ in surficial structural character in the following respects:

1. Folds exposed at the surface in the Del Rio thrust sheet are less uniform in trend and express more intense deformation than folds exposed at the surface in the Buffalo Mountain thrust sheet with the exception of the Paint Creek syncline.

2. Thrust faults within the Del Rio thrust sheet do not dip so

steeply as thrust faults within the Buffalo Mountain thrust sheet, and in addition they are warped. Their sub-horizontal, warped nature is indicated by small windows and by erratic traces.

Factors contributing to the surficial structural differences between the two thrust sheets are:

1. The Del Rio thrust sheet apparently wedges out from the base upward northeastward in the southwestern Bald Mountains, pinching out beneath the southwest end of the Buffalo Mountain thrust sheet.

2. The northeastern end of the Del Rio thrust sheet was overridden and presumably bevelled by the Buffalo Mountain thrust sheet.

3. Surface drainage in the Del Rio thrust sheet, more highly developed than in the Buffalo Mountain thrust sheet, has dissected and thinned the Del Rio thrust sheet to a greater extent than the Buffalo Mountain thrust sheet.

Thrust faults within the Buffalo Mountain thrust sheet probably flatten at depth before intersecting the Buffalo Mountain thrust fault. Both the Buffalo Mountain and Del Rio thrust sheets are deformed most at their bases by folds and small-scale thrust faults that attenuate upward. The northeasternmost exposed portion of the Del Rio thrust sheet is probably a surface representation of the structural nature of the Buffalo Mountain thrust sheet at depth.

The Buffalo Mountain thrust sheet is synclinal in structure in the southwestern Bald Mountains; synclines have been faulted and imbricated.

REFERENCES CITED

Bearce, D. N., 1966, Geology of the Chilhowee Group and the Ocoee Series in the Southwestern Bald Mountains, Greene and Cocke Counties, Tennessee: Dissertation unpublished, University of Tennessee.

Ferguson, H. W., and Jewell, W. B., 1951, Geology and barite deposits of the Del Rio District, Cocke County, Tennessee: Tenn. Div. Geol. Bull. 57, 228 p.

Keith, A., 1895, Description of the Knoxville sheet (Tennessee-North Carolina): U. S. Geol. Survey Atlas, Knoxville Folio (No. 16), 6 p., maps.

_____, 1903, Description of the Cranberry Quadrangle (North Carolina-Tennessee): U. S. Geol. Survey Atlas, Cranberry Folio (No. 90), 9 p., maps.

_____, 1904, Description of the Asheville Quadrangle (North Carolina-Tennessee): U. S. Geol. Survey Atlas, Asheville Folio (No. 116), 10 p., maps.

_____, 1905, Description of the Greeneville Quadrangle (Tennessee-North Carolina): U. S. Geol. Survey Atlas, Greeneville Folio (No. 118), 8 p., maps.

Keith, A., 1907, Description of the Roan Mountain Quadrangle (North Carolina-Tennessee): U. S. Geol. Survey Atlas, Roan Mountain Folio (No. 151), 8 p., maps.

King, P. B., 1949, The Base of the Cambrian in the Southern Appalachians: Am. Jour. Sci., v. 257, 1. 513-530, 622-645.

King, P. B., 1964, Geology of the Central Great Smoky Mountains, Tennessee: U.S. Geol. Survey Prof. Paper 349-C, p. 1-148.

King, P. B., Ferguson, H. W., Craig, L. C., and Rodgers, J., 1944, Geology and manganese deposits of Northeast Tennessee: Tenn. Div. Geology Bull. 52, 275 p.

King, P. B., Hadley, J. B., Neuman, R. B., and Hamilton, W., 1958, Stratigraphy of Ocoee Series, Great Smoky Mountains, Tennessee and North Carolina: Geol. Soc. America Bull., v. 69, p. 947-966.

Laurence, R. A., and Palmer, A. R., 1963, Age of the Murray Shale and Hesse Quartzite on Chilhowee Mountain, Blount County, Tennessee: U. S. Geol. Survey Prof. Paper 475-C, p. 53-54.

Ordway, R. J., 1959, Geology of the Buffalo Mountain-Cherokee Mountain area in Northeastern Tennessee: Geol. Soc. America Bull., v. 70, p. 619-636.

Oriel, S. S., 1949, Geology and mineral resources of the Hot Springs Window, Madison County, North Carolina: Dissertation unpublished, Yale University.

Rodgers, J., 1953, Geologic map of East Tennessee with explanatory text: Tenn. Div. Geology Bull. 58, 158 p.

Safford, J. M. 1869, Geology of Tennessee: Nashville, 550 p.

Shekarchi, E., 1959, The Geology of the Flag Pond Quadrangle, Tennessee-North Carolina: Dissertation unpublished, University of Tennessee.

Stose, G. W., and Stose, A. J., 1944, The Chilhowee Group and Ocoee Series of the Southern Appalachians: Am. Jour. Sci., v. 242, p. 367-390, 401-416.

PHOSPHOSIDERITE ASSOCIATED WITH NELSONITE ROCK IN NELSON COUNTY, VIRGINIA

By

Richard.S. Mitchell
University of Virginia

ABSTRACT

Greenish cryptocrystalline phosphosiderite occurs in hydrothermally altered ilmenite-nelsonite dike rocks in Nelson County, Virginia. Strengite, dimorphous with phosphosiderite, also occurs but it is much rarer. Indexed X-ray powder data are given for both minerals. In addition to ilmenite and apatite which are essential to the nelsonite, associated minerals are talc, chlorite, anatase, and wavellite.

INTRODUCTION

The relatively rare mineral phosphosiderite (also called metastrengite or clinostrengite) occurs in altered ilmenite-nelsonite dike rocks in Nelson County, Virginia. Although the mineral has not been reported from the area previously it was referred to by Watson and Taber (1913, p. 106) as an unknown "compound of bluish-green color." A recent examination of nelsonite specimens in Lewis Brooks Museum (University of Virginia), as well as new materials in the field, has shown that phosphosiderite is quite common, especially at one locality near Jonesboro.

DATA FOR PHOSPHOSIDERITE

Green to bluish-green cryptocrystalline phosphosiderite occurs in nelsonite either as thin crusts with small botryoidal structures, or as seam fillings, or intimately associated with talc as powdery coatings. The mineral is brittle, has a conchoidal fracture, a hardness of 4.5, and a pale greenish-yellow streak. Thin fragments are translucent.

A pure sample of phosphosiderite was submitted for semiquantitative spectrographic analysis. The chief elements detected are iron and phosphorous. Trace amounts of numerous other elements were found, but only Al_2O_3, 1.5 percent, and TiO_2, 0.75 percent, are significant. This analysis verified phosphosiderite and eliminated any

possibility that the mineral might be the aluminum analog metavariscite, or some other closely related mineral.

Initially the mineral was identified from X-ray powder films. The measured interplanar spacings given in Table 1 represent the average of values obtained from four films of four different samples, made with CuKα radiation in cameras with 11.46 cm diameters. In order to index the reflections all interplanar spacings allowed down through 2.27Å were calculated from the following monoclinic data of McConnell (1939, 1940): a = 5.30 Å, b = 9.79 Å, c = 8.67 Å, β = 90.6°, $P2_1/n$. In his earlier paper McConnell (1939) gave calculated interplanar spacings, but the indexing is not entirely correct because the space group was not certain at that time. The $P2_1/n$ symmetry (McConnell, 1940) requires that hO1 reflections be absent when h + 1 is odd and that OkO be absent when k is odd. The observed X-ray powder data for the Nelson County phosphosiderite compare well with those of Neves (1958), Wilk (1959/60), Kahler (1962), and Arlidge et al. (1963), and are conformable to the structure of the mineral recently determined by Moore (1966). Impurity lines of some X-ray films were shown to belong to trace amounts of the dimorphous mineral strengite, an observation also made by McConnell (1939).

ASSOCIATED STRENGITE

Strengite was discernible on two specimens where it is closely associated with phosphosiderite. The strengite is light gray and has a dull to greasy luster. It occurs as masses, or as crusts and cavity fillings with small botryoidal development. Identification was based on X-ray powder data. The measured data in Table 2 represent averaged values obtained from four films (CuKα radiation, 11.46 cm diameter cameras). The calculated data represent all possible values through 2.27 Å based on the orthorhombic cell reported on ASTM powder diffraction data card 15-513: a = 10.05 Å, b = 9.92 Å, c = 8.74 Å, Pcab. Moore (1966) who has studied the structural relationships between strengite and phosphosiderite has pointed out that these dimorphous minerals commonly occur together.

OCCURRENCE

The Nelson County phosphosiderite and strengite were first noticed on specimens (V4081, V4183) in Lewis Brooks Museum. Unfortunately the exact localities for these specimens are not known. A visit was made to the Roseland area where there are numerous nelsonite dikes (Watson and Taber, 1913; Ross, 1941; Hillhouse, 1960). Although several outcrops were examined phosphosiderite and strengite were found only in nelsonite on the Edwin Hughes farm a short distance

Table 1. X-ray powder data for phosphosiderite, Nelson County, Virginia. Filtered copper radiation. Cameras of 11.46 cm diameter.

hkl	d (calc.)Å	d (meas.)Å	I (obs.)
011	6.49	6.50	mw
020	4.90	4.93	m+
110	4.66	4.66	m+
$\bar{1}01$	4.54		
101	4.50		
002	4.34	4.36	vs
021	4.26		
$\bar{1}11$	4.12		
111	4.09	4.10	vw
012	3.96		
120	3.60	3.60	ms
$\bar{1}21$	3.33	3.32	vvw
121	3.31		
022	3.25		
$\bar{1}12$	3.19		
112	3.16		
031	3.05		
130, $\bar{1}22$	2.78	2.78	ms
013	2.77		
122	2.76		
$\bar{1}31$, 200	2.65	2.65	vvw
131	2.64		
032	2.61		
210	2.56		
$\bar{1}03$	2.55	2.55	ms
103	2.53		
023	2.49		
$\bar{1}13$	2.47		
$\bar{2}11$	2.46		
040, 211, 113	2.45	2.44	vvw
041	2.36		
$\bar{1}32$	2.35	2.35	vvw
132, 220	2.33		
$\bar{2}02$	2.27	2.27	vvw
		2.12	vvw
		2.07	vvw-
		2.01	w
		1.81	vvw
		1.76	vvw
		1.71	vvw
		1.66	vvw

Table 2. X-ray powder data for strengite, Nelson County, Virginia. Filtered copper radiation. Cameras of 11.46 cm diameter.

hkl	d (calc.)Å	d (meas.)Å	I (obs.)
111	5.49	5.51	m
200	5.03		
020	4.96	4.94	mw-
120	4.45		
002	4.37	4.38	ms
201	4.36		
012, 211	3.99	3.98	mw-
121	3.96		
112	3.72	3.72	vw
220	3.53		
202	3.30		
022	3.28	3.28	vvw
221	3.27		
212	3.13		
122	3.12	3.11	mw
311	2.98	3.00	w
131	2.96	2.94	w
320	2.78		
222	2.75		
113	2.69		
321	2.65		
032	2.64		
231	2.63	2.62	vvw
312	2.57		
132	2.55	2.54	mw
203	2.52		
400	2.51		
040	2.48		
213, 123	2.44	2.45	vw
401, 140	2.41		
411	2.35	2.36	vvw
322	2.34		
232	2.33		
141	2.32		
331	2.27	2.28	vvw
		2.13	vw
		2.08	vvw
		2.00	vw
		1.96	vvw
		1.76	vvw
		1.72	vvw
		1.65	vw

southeast of Jonesboro. Float pieces are common near the barn, and very rich phosphosiderite specimens occur in place at a deep roadcut in the barnyard.

Bright green phosphosiderite covers large joint planes of the nelsonite rock. In addition to porcelaneous masses, often with small botryoidal surfaces, the mineral also occurs as narrow veins in the nelsonite, and as cellular replacements of apatite grains in the rock, and very commonly mixed with talc to form light green powdery surfaces on the rock. Very thin bluish-white, white, and tan crusts overlying deep emerald-green phosphosiderite crusts were shown by X-ray study also to be phosphosiderite. Strengite is very rare at the Hughes farm. Here it occurs as light gray greasy masses and crusts with botryoidal development within the small subspherical cavities formerly occupied by apatite grains in nelsonite.

In addition to ilmenite and apatite, which are the essential minerals of the nelsonite matrix rock, talc is the most common associated mineral at the Hughes locality. It occurs as earthy to micaceous masses and especially as coatings on joint planes. Individual plates up to 2.5 mm across were noticed. It varies from white to green, the green being due to admixed phosphosiderite. Yellowish micaceous chlorite occurs in some specimens. One nelsonite piece was found in which black ilmenite is replaced by greenish-brown anatase in such a way as to retain the original texture of the rock. In this one the essential apatite was not appreciably changed. In many other specimens, however, apatite is deeply etched and altered. Fine-grained white wavellite, stained brown, was found on some weathered spongelike nelsonite masses from which the apatite was removed. The writer has been unable to identify some additional minerals, one a thin yellowish-green botryoidal crust and another a small globule of white radiating needles.

Phosphosiderite and strengite have obviously formed from the alteration of nelsonite, iron coming from ilmenite and phosphate from apatite. The close association of these minerals with talc suggests that the alteration was hydrothermal. Studies of nelsonite dikes also led Hillhouse (1960, p. 124) to conclude that slight hydrothermal activity continued after the deposition of the dikes and resulted in the alteration of nelsonite minerals. However, he did not mention the secondary phosphates described here. In contrast, the writer did not find phosphosiderite in the numerous very weathered float specimens of nelsonite he examined.

REFERENCES CITED

Arlidge, E. Z., Farmer, V. C., Mitchell, B. D., and Mitchell, W. A., 1963, Infra-red, X-ray and thermal analysis of some aluminum and ferric phosphates: Jour. Appl. Chem., v. 13, p. 17-27.

Hillhouse, D. N., 1960, Geology of the Piney River-Roseland titanium

area, Nelson and Amherst Counties, Virginia: Ph. D. Dissert., Va. Polytech. Inst., 129 p.

Kahler, E., 1962, Sekundare Phosphate von der Koralpe, Steiermark: Neues Jahrb. Mineralogie Abh., v. 98, p. 1-13.

McConnell, D., 1939, Symmetry of phosphosiderite: Am. Mineralogist, v. 24, p. 636-642.

_____, 1940, Clinobarrandite and the isodimorphous series, variscite-metavariscite: Am. Mineralogist, v. 25, p. 719-725.

Moore, P. B., 1966, The crystal structure of metastrengite and its relationship to strengite and phosphophyllite: Am. Mineralogist, v. 51, p. 168-176.

Neves, J. M. C., 1958, Novos minerais dos pegmatitos de Mangualke (Portugal): Univ. Coimbra mus. e lab. mineralog. e geol. e contro estudos geol. Mems. e noticias, no. 46, p. 56-67.

Ross, C. S., 1941, Occurrence and origin of the titanium deposits in Nelson and Amherst Counties, Virginia: U. S. Geol. Survey Prof. Paper 198, 59 p.

Watson, T. L., and Taber, S., 1913, Geology of the titanium and apatite deposits of Virginia: Va. Geol. Survey Bull., v. 3A, 308 p.

Wilk, H., 1959/60, Phosphosiderit und Strengit von Pleystein in Ostbayern: Acta Albertina Ratisbonensia, v. 23, p. 107-170.

SOUTHEASTERN GEOLOGY

AUTHOR-SUBJECT INDEX

VOLUME 1 - 10
1959 - 1969

Compiled By
Jane Tyndall

TABLE OF CONTENTS

Volume Issue Article	
3. 1. 1	Rock Analyses in the Carolina Slate Belt and the Charlotte Belt of Newberry County, South Carolina
3. 1. 2	The Stratigraphic Paleontology of the Chickamauga Group of the Red Mountain Area, Alabama
3. 1. 3	Recent Root Casts in Sediments of the Apalachicola Delta, Florida
3. 2. 1	A Biostratigraphic Evaluation of the Snow Hill Member, Upper Cretaceous of North Carolina
3. 3. 1	A Review of Regional Heavy-Mineral Reconnaissance and its Application in the Southeastern Piedmont
3. 3. 2	Environmental Studies of the Cretaceous Mount Laurel and Wenonah Sands of New Jersey
3. 3. 3	The Sediments of the Beaufort Inlet Area, North Carolina
3. 4. 1	Bouguer Gravity Map of North Carolina
3. 4. 2	Airborne Radioactivity Surveys -- A Geologic Exploration Tool
3. 4. 3	Geology of the Elk Knob Copper Deposit and Vicinity, Watauga County, North Carolina
4. 1. 1	A Supplementary Catalog of Type Localities of Coastal Plain Stratigraphic Units
4. 1. 2	The Beaufort, South Carolina, Magnetic Low
4. 2. 1	Digital Computer Program for Identification of Minerals by X-ray Diffraction
4. 2. 2	Geomorphology and the Sediment Transport System
4. 3. 1	Paleoecology of the Pamlico Formation (Late Pleistocene): Nixonville Quadrangle, Horry County, South Carolina
4. 3. 2	Rocks of the Carolina Slate Belt in Orange County, North Carolina
4. 4. 1	Configuration of the Cretaceous-Tertiary Boundary in the Delmarva Peninsula and Vicinity
4. 4. 2	Nature and Origin of the Slump Structures in the Black Mingo Formation of South Carolina
4. 4. 3	Stratigraphy of the Neogene Deposits, Lower Neuse Estuary, North Carolina
4. 4. 4	Table of d Spacings from 2.000° to 60.975° 2θ in 0.025 Degree Increments Copper $K\alpha$ Radiation
5. 1. 1	A Report on Geological and Ground-Water Investigations in Pigeon Roost Watershed, Marshall County, Mississippi
5. 1. 2	The Cretaceous-Tertiary Boundary at the Type Locality of the Castle Hayne Formation
5. 1. 3	Paleoecology of the Type Waccamaw (Pliocene?) Outcrops: South Carolina
5. 2. 1	Isolated Fault Scarps on the Continental Slope of Southwest Florida
5. 2. 2	Pleistocene "Coquina" at 20th Avenue South Myrtle Beach, South Carolina, and other Similar Deposits
5. 2. 3	Chemical Analyses of Rocks of the Carolina Slate Belt
5. 2. 4	Filled Submarine Spring Vents in Cretaceous Rocks of Alabama
5. 3. 1	Rock-Stratigraphic Distribution of the Surry Scarp in Central South Carolina
5. 3. 2	Gravity Studies in the Concord Quadrangle, North Carolina
5. 3. 3	Notes on Marine Geology off the Mouth of the North Edisto River, North Carolina
5. 4. 1	Hydrogeologic Framework of the Gulf and Atlantic Coastal Plain
5. 4. 2	The Pungo River Formation, a New Name for Middle Miocene Phosphorites in Beaufort County, North Carolina
5. 4. 3	An Unusual Radioactive, Rare Earth-bearing Sulfide Deposit in Cabarrus County, North Carolina
5. 4. 4	The Elberton Batholith

Volume Issue Article	
6. 1. 1	Clay Mineral Assemblages in a South Carolina Lake-River, Estuary Complex
6. 1. 2	Beach Profiles of a Georgia Barrier Island
6. 1. 3	Geologic Section Along a Carolina Bay, Sumter County, S. C.
6. 1. 4	Barrier-and-Lagoon Sets on High Terraces in the Florida Panhandle
6. 1. 5	Geomorphic Elements of the Area between the Cape Fear and Pee Dee Rivers, North and South Carolina
6. 2. 1	Areal Modal Variation in the Farrington Igneous Complex, Chatham and Orange Counties, North Carolina
6. 2. 2	Virginia Metamict Minerals: Comments on a Uranium-Niobium Oxide from Powhatan County
6. 2. 3	Compositions of Minerals Within the Wall Rocks of a Granitic Batholith
6. 3. 1	Geology of the Carolina Slate Belt West of the Deep River-Wadesboro Triassic Basin, North Carolina
6. 3. 2	The Use of X-ray Diffraction for the Quantitative Analysis of Naturally Occurring Multicomponent Mineral Systems
6. 3. 3	Bathymetry of the Miami Terrace
6. 3. 4	The Stratigraphic Significance of an Upper Miocene Fossil Discovery in Jefferson County, Florida
6. 4. 1	Frequencies of Infaunal Invertebrates Related to Water Content of Chesapeake Bay Sediments
6. 4. 2	Laumontite-Leonhardite from Durham County, N. C.
6. 4. 3	Ultramylonite Zones in the Western Carolinas
6. 4. 4	Petrography of the Soapstone Deposits near Old Dominion, Albemarle County, Virginia
6. 4. 5	Marine Terraces: Pre-Pleistocene(?)
7. 1. 1	The General Absence of Blue Quartz in Sedimentary Rocks of the "Folded Appalachians" of Southwestern Virginia
7. 1. 2	Notes on Technique for Sampling Suspended Sediments
7. 1. 3	Bottom Topography of the Georgia Continental Shelf
7. 1. 4	Submerged Beach on a Zero-Energy Coast
7. 1. 5	Abundance of Pollen and Spores in Marine Sediments off the Eastern Coast of the United States
7. 1. 6	Faulted Alluvial and Colluvial Deposits Along the Blue Ridge near Saluda, North Carolina
7. 2. 1	The Surry Scarp from Fountain to Potters Hill, North Carolina
7. 2. 2	Clay Mineralogy, Stratigraphy, and Structural Setting of the Hawthorn Formation, Coosawhatchie District, South Carolina
7. 2. 3	Sediments of the Choptank River, Maryland
7. 2. 4	Stratigraphy of the Jackson Group (Eocene) in Central Georgia
7. 3. 1	Trace Metals in Quartz by Atomic Absorbtion Spectrophotometry
7. 3. 2	Geomorphology of River Valleys in the Southeastern Atlantic Coastal Plain
7. 3. 3	Paragonite-bearing Phyllites in the Central Virginia Piedmont
7. 3. 4	The Midway-Wilcox Boundary in Kemper and Lauderdale Counties, Mississippi
7. 3. 5	Porosity Index
7. 3. 6	Notes on Five Marine Pleistocene Localities in Northeastern North Carolina
7. 4. 1	The Clay Minerals of a Traverse on the North Carolina Continental Margin and Bermuda Rise
7. 4. 2	Density Sorting as Indicated by Departure from Gaussian Curve
7. 4. 3	Coastal Plain Stratigraphy and Geomorphology near Benson, North Carolina
7. 4. 4	Virginia Metamict Minerals: Allanite

Volume Issue Article	
8. 1. 1	Sea-floor Strength Observations from the DRV Alvin in the Tongue of the Ocean, Bahamas
8. 1. 2	Nickeliferous Soils and Stream Sediments Associated with Peridotites near Democrat, North Carolina
8. 1. 3	Redefinition of the Hillabee Schist, Alabama
8. 1. 4	North Carolina Shelf Phosphate Deposit of Possible Commercial Interest
8. 2. 1	Chloritoid from Orange County, North Carolina
8. 2. 2	The Ripple Mark Analog: Preliminary Results
8. 2. 3	The Diabase of the Butner-Creedmoor Area, Granville County, North Carolina
8. 2. 4	A Pliocene Tennessee River Hypothesis for Mississippi
8. 2. 5	On Suspended Sediment Sampling by Filtration
8. 2. 6	Geomorphology of River Valleys in the Southeastern Atlantic Coastal Plain: A Discussion
8. 2. 7	General Relationships between Soil and Environments on the Southern Atlantic Coastal Plain: A Reply
8. 3. 1	The Salisbury Adamellite Pluton, North Carolina
8. 3. 2	Outcrop of the Yorktown Formation (Upper Miocene) in Onslow Bay, North Carolina
8. 3. 3	The Effect of Minor Changes of Emission Wavelength in Quantitative X-ray Analysis
8. 3. 4	Virginia Metamict Minerals: X-ray Study of Fergusonite
8. 4. 1	The Continental Margin South of Cape Hatteras, North Carolina: Shallow Structure
8. 4. 2	The Physiography of Sequatchie Valley and Adjacent Portions of the Cumberland Plateau, Tennessee
8. 4. 3	Potential Uses of Flow Net Analysis in Watershed Engineering
9. 1. 1	The Precipitation of Metastable Carbonate Minerals at Low Temperature and Pressure
9. 1. 2	Loess in Southcentral Louisiana
9. 1. 3	Ground Water Chemistry as a Tool for Geologic Investigation in the Southeastern Piedmont
9. 1. 4	Relationship between Coastal Landforms and Size Distribution of Surficial Sediments, Horry and Marion Counties, South Carolina
9. 2. 1	Mineral Facies in the Tertiary of the Continental Shelf and Blake Plateau
9. 2. 2	A New Chronology for Braided Stream Surface Formation in the Lower Mississippi Valley
9. 2. 3	Observations on the Distribution of Sands Within the Potomac Formation of Northern Delaware
9. 2. 4	The Piezometric Surface of the Coastal Plain Aquifer in Georgia, Estimates of Original Elevation and Long-Term Decline
9. 2. 5	The Pleistocene Geology of Princess Anne County, Virginia
9. 3. 1	A Proposal for Coordinating Geological Research in the Southeast
9. 3. 2	Structure of Easternmost North Carolina Piedmont
9. 3. 3	Spilitic Amygdaloidal Basal Flow Rocks and Associated Pillow Structure in Orange County, North Carolina
9. 3. 4	Barian Florencite, Weinschenkite, and Rhabdophane from a Perrierite-Bearing Pegmatite in Amherst County, Virginia
9. 3. 5	Mineralogy of Chlorite-Talc Schist from Washington, D. C.
9. 3. 6	Bryozoan Paleoecology from the Tertiary of Alabama
9. 3. 7	A Bored Ectoproct from the Middle Mississippian of Tennessee
9. 3. 8	Research Inquiry
9. 4. 1	Shallow Structure of Continental Shelves and Slopes
9. 4. 2.	Quaternary and Shelf Sediments of Georgia
9. 4. 3	Deeper Subsurface Waters Along the Atlantic Continental Margin

AUTHOR INDEX

SUBJECT INDEX

(Volume, Issue, Article)